

Analysis of tropospheric transport in the Pacific Basin using the adjoint technique

Tomislava Vukićević

Cooperative Institute for Research in the Atmosphere, Colorado State University, Fort Collins

Peter Hess

National Center for Atmospheric Research, Boulder, Colorado

Abstract. An adjoint sensitivity analysis is performed within a regional episodic chemical transport model covering the Pacific Basin. The analysis is performed with respect to the concentration over Hawaii of a soluble and insoluble chemically inert species, with the same emissions as NO_x . The sensitivity is examined at times of elevated tracer mixing ratio at 300, 680, and 900 mbar. The sensitivity to the average mixing ratio at 680 mbar is also examined. The meteorological conditions of April and May 1992 are used for the transport. The adjoint analysis includes the effect of the entire model transport function. It provides a method to analyze the transport of modeled emissions to Hawaii, including the effect of various emission regions, and the associated transport pathways and timescales. The boundary layer mixing ratio at Hawaii is most sensitive to local emissions, with emissions from North America and Asia also contributing to the modeled concentration. In the free troposphere the concentration over Hawaii is most sensitive to emissions from Asia. The adjoint also allows modeled processes to be ranked by their importance in determining the concentration of a species at a particular location. At Hawaii, emissions are ranked first and second in order of importance for the insoluble and soluble species, respectively. For the soluble species the solution is most sensitive to the modeled wet deposition by nonconvective rain. Free tropospheric mixing is generally next in order of importance. Deep convection is important in some locations, particularly for the 300 mbar concentrations. Boundary layer processes, including dry deposition, are generally not important to the free tropospheric solution at Hawaii.

1. Introduction

The speciation and geographic distribution of chemical emissions is changing due to economic and sociological factors associated with population growth, new technologies, and continued industrialization and urbanization. The associated changes to tropospheric chemical composition are profound. The relation between emissions and tropospheric composition is largely determined by the chemical transformations and physical loss processes along transport pathways.

Significant transport away from emission regions can occur in the boundary layer but is relatively slow and susceptible to rainout and surface deposition. In the free troposphere, surface deposition and rainout are reduced, and transport to global scales is more rapid. However, emissions are often lofted from the boundary layer to the free troposphere by convection and synoptic lifting, processes frequently associated with precipitation. Consequently, the transport of soluble species to the middle and upper troposphere can be rather inefficient.

The transport pathway also affects the chemistry directly. For example, the chemistry of the upper and lower troposphere is distinctly different [e.g., Davis *et al.*, 1996]. The photochemical lifetime of NO_x increases by almost a factor of 10 between the boundary layer and the upper troposphere [Ehhalt

et al., 1992], and in the upper troposphere NO_x can be more effective at producing ozone than at the surface [Liu *et al.*, 1987; Pickering *et al.*, 1992a, b; Davis *et al.*, 1996]. The rainout of soluble species also affects the chemistry, driving it from its local photochemical equilibrium and thereby driving rapid chemical transformations.

The Pacific Ocean is the largest pristine location in the Northern Hemisphere, although cities along the Pacific Rim are growing rapidly. A number of field campaigns (e.g., the Pacific Exploratory Mission-West, Phase A and B [Hoell *et al.*, 1996, 1997]) have examined the outflow from Asia over the western Pacific. The Mauna Loa Observatory Photochemistry Experiment (MLOPEX) [Atlas and Ridley, 1996] field campaign sampled older, more processed air. This campaign sampled the annual cycle of a wide variety of constituents at the Mauna Loa Observatory (MLO), located at approximately 680 mbar on the island of Hawaii. This location is one of the most remote regions of the Northern Hemisphere (N.H.), approximately 4000 km from Tokyo and 2500 km from Los Angeles.

This paper describes an application of the adjoint technique to an analysis of pollutant transport to Hawaii from chemical emissions on the Pacific Rim. The adjoint technique is used to diagnose the transport of a chemically inert and insoluble species, and an inert, but soluble species, to Hawaii from emission sources within the greater Pacific Basin. The relative importance of chemical emissions, chemical losses through rainout and surface deposition, boundary layer transport, and advective and convective transport in determining the concentration

Copyright 2000 by the American Geophysical Union.

Paper number 1999JD901110.
0148-0227/00/1999JD901110\$09.00

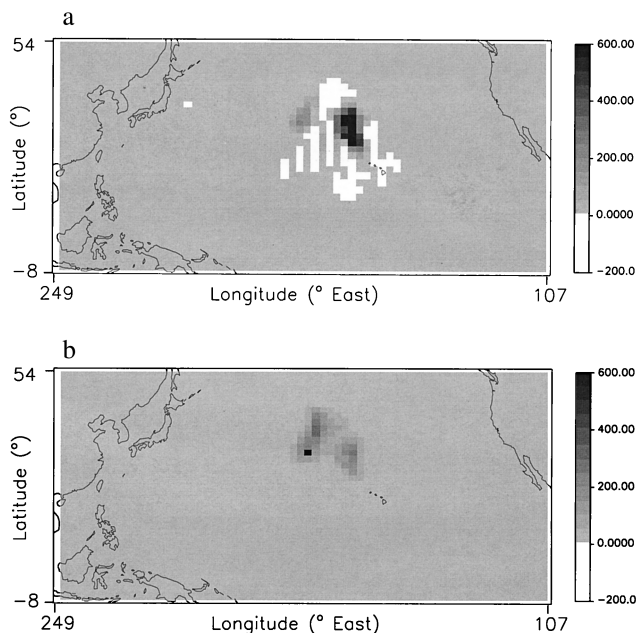


Figure 1. Adjoint model solution for NOYI (pptv) using different advection algorithms: (a) linear MPDATA and (b) donor cell.

of pollutants at Hawaii is examined. The adjoint technique provides the formalism to measure the impact of each of these processes to the pollutant transport to Hawaii. Chemical transformations are not addressed in this study. Instead, we focus on the sensitivity of species concentrations to their particular emissions and transport pathways.

2. Chemical Transport Model

The adjoint sensitivity method requires an initial integration of a transport model to produce the basic state solution. The adjoint technique is then applied to evaluate the sensitivity of a particular feature of this solution to model parameters, initial conditions, and boundary conditions. The integration and the associated model (named HANK) are described in detail by P. G. Hess et al. (Modeling the chemistry and transport in the Pacific Basin during the spring MLOPEX intensive with the National Center for Atmospheric Research chemical transport model, submitted to *Journal of Geophysical Research*, 1999, hereinafter referred to as Hess et al., submitted manuscript, 1999). A brief description of the model is repeated here.

HANK is an episodic, limited domain, chemical transport model. It is driven by time-averaged output fields from the Pennsylvania State University/National Center for Atmospheric Research (PSU/NCAR) Mesoscale Modeling System (MM5). The fields are averaged over 3 hours, and they are an unweighted average except for the convective fields. The convective fields are weighted by the convective mass flux. The MM5 is a part of a regional modeling system [Anthes and Warner, 1978], described by Grell et al. [1993], which solves the primitive equations within a regional domain. The MM5 includes a complete set of physical parameterizations. The initial and lateral boundary conditions for the MM5 are analyzed meteorological fields. The resolution used in HANK and MM5 is 243 km on a Mercator projection in the horizontal, with 23 model layers between the surface and 100 mbar in the vertical.

The vertical grid is in sigma coordinates with approximately 40 to 50 mbar resolution in the middle and upper troposphere and seven levels below, 800 mbar.

While chemistry was included by Hess et al. (submitted manuscript, 1999), this study examines the transport of inert species subject only to surface emissions, surface deposition, and washout. The model without chemical interactions can be symbolically represented as

$$\frac{\partial \chi}{\partial t} = \mathcal{T}(\chi) + \mathcal{W}(\chi) \quad (1)$$

where $\chi(x, t)$ is the species mixing ratio within the model domain, x is the spatial coordinate, t is time, and \mathcal{T} and \mathcal{W} are the transport and wet deposition operators. Emissions are included in the transport operator as part of the lower boundary condition.

We seek a solution of this system in a limited domain (see Figure 1a) subject to prescribed initial conditions (χ_0) and boundary conditions (χ_b). In addition, the transport and deposition operators contain a number of “free” physical parameters α whose values are input from the MM5. These parameters are either two- or three-dimensional fields and are generally time-varying (except for the model emissions). The solution depends on these parameters. The nine parameters examined in this study are listed in Table 1 and discussed below.

The transport operator \mathcal{T} includes the following process: advective tracer transport using the Smolarkiewicz advection scheme [Smolarkiewicz, 1984]; deep convection and shallow convection transport using the Grell parameterization, a modified Arakawa-Schubert scheme [Grell, 1993]; and vertical diffusion in conjunction with the Holtslag boundary layer transport parameterization [Holtslag and Moeng, 1991]. The wet deposition operator \mathcal{W} includes removal of species by wet deposition.

The Smolarkiewicz [1984] advection scheme is a second-order, positive definite, and conservative scheme, designated Multidimensional Positive Definite Advection Transport Algorithm (MPDATA). It first advects the tracer field with the MM5 winds, then performs subsequent iterative advective steps to correct for the excessive diffusivity. The subsequent steps are nonlinear with respect to the tracer mixing ratio, even though the actual advective process is linear. Nonlinearity is a common attribute of numerical advective schemes [Hecht et al., 1995; Roe and Sidilkover, 1992], as the monotonicity of the solution cannot be maintained with linear schemes [Godunov, 1959; Smolarkiewicz and Margolin, 1999]. Species concentrations are specified at the lateral boundaries. This lateral boundary condition is included in the advective operator.

The deep and shallow parameterized convection differ in their assumed entrainment and detrainment rates, and in the inclusion of a convective downdraft in the deep convective clouds. No entrainment or detrainment is assumed to occur in the updraft plume of deep convection. In contrast, shallow convective clouds rapidly mix with their environment between cloud bottom and cloud top, with equal entrainment and detrainment rates. The sensitivity of the model solution to deep and shallow convective clouds is examined through the sensitivity to the updraft mass flux.

Turbulent transport in the boundary layer is parameterized by vertical diffusion and a nonlocal transport term:

Table 1. Parameters and Influence Categories

Process	Parameters	Acronyms	Categories of Influence	Index
Deep convection	mass flux, $\frac{\text{kg}}{\text{m}^2 \text{ s}}$	DCMF	PDCMF (positive)	1
			NDCMF (negative)	2
Shallow convection	mass flux, $\frac{\text{kg}}{\text{m}^2 \text{ s}}$	SCMF	PSCMF (positive)	3
			NSCMF (negative)	4
Dry deposition	deposition velocity, $\frac{\text{m}}{\text{s}}$	DV	NDV (negative)	5
Top boundary condition	top boundary value, $\frac{\text{molecules} - \text{species}}{\text{molecules} - \text{air}}$ (concentration)	TBV	PTBV (positive)	6
Emission	emission, $\frac{\text{molecules}}{\text{m}^2 \text{ s}}$	EMF	PEMF (positive)	7
Wet deposition	convective rain rate, $\frac{\text{kg}}{\text{m}^2 \text{ s}}$	CR	NCR (negative)	8
	nonconvective rain rate, $\frac{\text{kg}}{\text{m}^2 \text{ s}}$	NCR	NNCR (negative)	9
Vertical Mixing	direct mixing coefficient, $\frac{\text{m}^2}{\text{s}}$	DMC	PDMC-fa (positive)	10
			NDMC-fa (negative)	11
			PDMC-pbL (positive)	12
			NDMC-pbL (negative)	13
	countergradient mixing coefficient, m^{-1}	CGMC	PCGMC (positive)	14
			NCGMC (negative)	15

$$\frac{\partial \chi}{\partial t} = \frac{1}{\rho} \frac{\partial}{\partial z} \left[\rho K_c \left(\frac{\partial \chi}{\partial z} - \gamma_c \right) \right] \quad (2)$$

where K_c ($\text{m}^2 \text{ s}^{-1}$) is the coefficient of vertical diffusivity and γ_c (m^{-1}) is the nonlocal transport term due to the large-scale boundary layer eddies which occur during convective and unstable conditions. The Holtslag boundary layer parameterization [Holtslag and Moeng, 1991] is used to determine the boundary layer depth, the diffusivities within the boundary layer, and the nonlocal transport term γ_c . Above the boundary layer the transport by vertical diffusion is of the same form as (2), but with $\gamma_c = 0$; the free tropospheric vertical diffusivity is determined using a parameterization based on the local Richardson number [Grell *et al.*, 1993] with a minimum vertical diffusivity of $1 \text{ m}^2 \text{ s}^{-1}$. The solution sensitivity is computed with respect to the vertical diffusivity K_c , and the nonlocal transport term γ_c (Table 1). Horizontal diffusion is not explicitly considered, although the numerics of the advection scheme results in an implicit diffusivity.

The upper and lower model boundary conditions are incorporated into the diffusive operator, and are therefore included in the transport operator \mathcal{T} . Species concentrations are specified at the upper model boundary, while a flux condition is specified at the lower boundary. Surface emissions and surface deposition are therefore included in the lower boundary condition. The sensitivity of the solution is computed with respect to surface emissions, dry deposition, and the upper boundary concentration (Table 1).

The surface deposition of chemical species is parameterized following Wesely [1989]. The dry deposition velocity is assumed to be inversely proportional to the sum of three resistances: the aerodynamic resistance explicitly calculated from the meteorological parameters output from MM5, the sublayer resistance dependent on the diffusivity of the species, and the bulk surface resistance which depends on the land surface, and the solubility and reactivity of the species in question.

Washout is modeled following Giorgi and Chameides [1985]. Washout does not occur in the nonprecipitating shallow convective clouds, but does occur in both the deep convective and resolved clouds. In both these cloud types the washout rate is

governed by the rain rate, the cloud microphysics, and the partitioning of species between the gaseous and aqueous phase as determined by the Henry's law effective equilibrium value. Resolved clouds are assumed to cover 100% of the grid. In deep convective clouds the effect of washout is incorporated directly into the convective parameterization. Soluble species are washed out as parcels are transported upward through the rainshaft. Since no detrainment or entrainment occurs in the parameterized cumulus updraft, washout only affects the species concentrations detrained at cloud top. Wet removal does not affect the species concentrations within the downdraft, as all rainwater is assumed to evaporate. In both convective and nonconvective clouds the sensitivity to washout is computed with respect to the rain rate (Table 1).

3. Adjoint Sensitivity Analysis

The adjoint technique is used to test particular aspects of a model solution to variations in model parameters, initial conditions, and boundary conditions. In this study we utilize the adjoint technique to examine the influence of all key controlling processes involved in the modeled episodic transport of chemical emissions to Hawaii. The adjoint technique has been used in a number of studies in meteorology to assess the impact of various processes on the model solution. These studies include an examination of the effect of selected processes on atmospheric blocking [Zou *et al.*, 1993], cyclogenesis [Rabier *et al.*, 1992; Vukićević and Raeder, 1995; Vukićević, 1998], and global tropospheric transport [Robertson, 1992; Marchuk, 1995; Pudykiewicz, 1998]. The adjoint method has also been used in global climate studies using simplified models [e.g., Hall *et al.*, 1982], and to examine the seasonal cycle of CO_2 as a function of surface fluxes [Kaminski *et al.*, 1996].

3.1. Theory

To evaluate the sensitivity of the basic state solution for the tracer mixing ratio χ , a general function of χ is used to characterize the solution of (1) over a particular area and time:

$$J(\chi) = \int_{\tau_1}^{\tau_2} \int_{\Omega} g(\chi) d\omega dt \quad (3)$$

where $[\tau_1, \tau_2]$ is the time interval examined, Ω is the spatial domain, $d\omega$ is the area differential, and $g(\chi)$ is a diagnostic operator. For example, the operator $g(\chi)$ might be the simulated species mixing ratio at a particular location x_0 and time t_0 (e.g., $g(\chi) = \chi(x, t) \delta(x - x_0) \delta(t - t_0)$, where δ represents the delta function). It might also be the weighted sum of the mixing ratio over a specific area and time period. Other more complex functions of χ are possible.

The sensitivity of the solution to variations in the controlling parameters (boundary conditions, initial conditions, or free parameters) is measured through changes in J . Using expression (3), this change is expressed as

$$\Delta J = \int_{\tau_1}^{\tau_2} \int_{\Omega} \left(\frac{\partial g}{\partial \chi} \right) \Delta \chi d\omega dt \quad (4)$$

where $\Delta \chi$ is the perturbation of the transport model solution due to variations in the controlling parameters. It is assumed in (4) that g is either a linear function of χ or that the variation of g and J are evaluated in the neighborhood of the unperturbed solution. In this study we use linear diagnostic functions.

The perturbation $\Delta \chi$ is related to the variations in controlling parameters via a perturbation transport model. We define the model to be linearized about the basic state. The resulting tangent linear model derived from equation (1) is

$$\left(\frac{\partial}{\partial t} - \mathcal{T}_\chi - \mathcal{W}_\chi \right) \Delta \chi = (\mathcal{T}_\alpha + \mathcal{W}_\alpha) \Delta \alpha. \quad (5)$$

Equation (5) describes the evolution of $\Delta \chi$, forced by a perturbation in the controlling parameters. This equation can be written succinctly as

$$L \Delta \chi = H_\alpha \Delta \alpha$$

where

$$L \equiv \frac{\partial}{\partial t} - (H_\chi)$$

and

$$H_\chi \equiv (\mathcal{T}_\chi + \mathcal{W}_\chi)$$

$$H_\alpha \equiv (\mathcal{T}_\alpha + \mathcal{W}_\alpha).$$

\mathcal{T}_χ and \mathcal{W}_χ are derivatives with respect to χ for the transport and deposition operators, and \mathcal{T}_α and \mathcal{W}_α are derivatives with respect to the free parameters for the same operators. These derivatives measure the linear local sensitivity of the basic state solution to perturbations, either in the tracer mixing ratio or the free parameters. L is the linear operator for the homogeneous perturbation model. The initial and boundary conditions for the perturbation model solution are defined as perturbations of the original initial and boundary conditions.

In practice we could evaluate ΔJ by perturbing the model controlling parameters and solving for $\Delta \chi$. This procedure is typically referred to as a forward sensitivity analysis. For each perturbation this method requires one model run. To characterize the actual sensitivity fields over the model phase space would require an integration of the original model for each

model grid point (the total number of grid points in the domain of integration is approximately 10^6 points) and for each time interval $[\tau, \tau_2]$.

The adjoint method offers a far more practical alternative to solve for ΔJ . This method involves finding the adjoint function χ^* . Given a change in a controlling parameter at position x_1 and time τ_1 , χ^* is a function which relates (or transfers) this change to the corresponding change in J (ΔJ). We also refer to the adjoint function χ^* as the transfer function. This function is defined for all model points and times. It is not necessary to recalculate $\Delta \chi$ through an additional integration for each desired perturbation. However, as we show below, the adjoint solution necessitates solving a differential equation to find the adjoint function χ^* . Once this function is found, the adjoint model produces the required sensitivity results in one integration. Its accuracy with respect to the forward sensitivity results is limited only by the linear assumption.

In the remainder of this section we briefly describe the adjoint function. This function describes how the solution sensitivity to varying the model controlling parameters, as measured by ΔJ , propagates backward in time through the model domain away from the region in which the solution sensitivity is measured (defined by g).

The required adjoint function is found by considering the adjoint operator. The adjoint to the differential operator L over the considered domain is defined as

$$\int_{\tau_1}^{\tau_2} \int_{\Omega} u L v d\omega dt = \int_{\tau_1}^{\tau_2} \int_{\Omega} v L^* u d\omega dt + BT. \quad (6)$$

This equation is derived through integration by parts, where u and v are bounded differentiable functions of the state variables, L^* is the adjoint operator to L , and BT represents the remaining terms after integration by parts, terms which depend on the boundary and initial conditions.

Integration by parts shows the form of L^* is

$$L^* \equiv -\frac{\partial}{\partial t} - (\mathcal{T}^* + \mathcal{W}^*_\chi) \quad (7)$$

where \mathcal{W}^*_χ and \mathcal{T}^*_χ are adjoint operators for \mathcal{W}_χ and \mathcal{T}_χ . The adjoint operator defines an adjoint equation for χ^* :

$$L^* \chi^* = \frac{\partial g}{\partial \chi} \quad (8)$$

The utility of using the expression (8) is seen by multiplying (5) by χ^* and (8) by $\Delta \chi$, subtracting and integrating over time and over the spatial domain (Ω) to give, after integration by parts,

$$\begin{aligned} \Delta J = & \int_{\tau_1}^{\tau_2} \int_{\Omega} (H_\alpha \Delta \alpha) \chi^* d\omega dt - \int_{\Omega} [\chi^* \Delta \chi]_{\tau_1}^{\tau_2} d\omega \\ & - \int_{\tau_1}^{\tau_2} [\chi^* \Delta \chi]_{\mathcal{C}(\omega)} dt \end{aligned} \quad (9)$$

where $\mathcal{C}(\omega)$ denotes the boundary of the integration domain. The lateral boundary conditions (lbc) for χ^* are dependent on the lbc in the forward model. In HANK we use the Diriclet condition. In the discrete formulation this produces outflow lbc in the adjoint solution. Equation (9) gives an alternative expression to (4) for ΔJ . The adjoint solution χ^* represents the

gradient of J with respect to initial and boundary conditions; H_α times χ^* is the gradient of J with respect to the parameters.

Note that whereas the forward sensitivity model is forced through a perturbation on the right-hand side of (5) (a perturbation in the model-controlling parameters), the adjoint equation is forced by $\partial g / \partial \chi$. Note that $\partial g / \partial \chi$ can be interpreted as the weight by which forward model solution ($\Delta \chi$) must be multiplied to give the model sensitivity (ΔJ) (equation (4)).

Adjoint analysis consists of determining the function (χ^*) from (8) at time $t < \tau_2$, and then using this function to analyze the relationship between the response of the system, as defined by ΔJ , and changes in the model solution parameters. The adjoint model equation (8) is integrated backward in time to solve for χ^* , as the partial time derivative in the adjoint equation has a negative sign (equation (7)). The adjoint “initial” condition must therefore be specified at $t = \tau_2$. Specifying $\chi^*(x, \tau_2) = 0$, allows the second term on the right-hand side of (9) to be expressed as

$$\int_{\Omega} \chi^*(\tau_1) \Delta \chi(x, \tau_1) d\omega. \quad (10)$$

This term transfers a perturbation in the tracer field at any position x within the model domain at any time $\tau_1 < \tau_2$ into the change in ΔJ through χ^* . For example, if $\chi(x_1, \tau_1)$ is changed by $\Delta \chi \delta(x - x_1)$, the associated change in J would be $\Delta \chi \chi^*(x_1, \tau_1)$. The adjoint solution also gives the sensitivity of the model solution to variations in the boundary conditions ($\Delta \chi|_{\partial(\omega)}$) through term 3. Similarly, the first term in (9) relates the change in J to the change in the model parameters ($H_\alpha \Delta \alpha$) through the model adjoint function.

3.2. Adjoint Operators in HANK

To develop an adjoint solution, HANK needs to be linearized. Typically, complex physical and dynamical models are linearized using the discrete model formulation rather than the continuous equations. A number of studies [Vukicevic, 1991; Vukicevic and Errico, 1993; Vukicevic, 1998; Zou et al., 1993; Kaminski et al., 1997] show that for large numerical models the discrete tangent linear and adjoint models are more accurate than the corresponding models developed from the continuous equations. This is due to their consistency with the original model formulation. The accuracy is defined here as the agreement between the model sensitivity evaluated with the forward model and that evaluated with the adjoint model.

The following specific processes are linearized in HANK: advection, transport by deep convection, transport by shallow convection, vertical mixing, dry deposition, wet deposition, and emissions. The continuous version of these operators are theoretically linear in χ , making H_χ identical to the original model operator. As transport and deposition are linear with respect to the tracer χ , the relationship between the model solution and the initial and boundary conditions (including emissions) is linear. Therefore the adjoint solution is valid for arbitrary perturbations in the initial conditions, boundary conditions, and in the emissions.

In practice, however, the discrete advection scheme MPDATA is nonlinear. Several different approaches can be taken to linearize this discrete advection operator. The first approach is to linearize MPDATA allowing variations in both the wind and in the tracer mixing ratio. Although this results in a linear advection scheme, the resulting scheme is not positive definite or conservative, attributes of the original scheme. Conse-

quently, over and under shoots of the adjoint function χ^* occur in the integration. An example of the corresponding adjoint solution is shown in Figure 1a.

To avoid this excessive noise, we linearize the advection equation about the tracer field only, neglecting variations in the wind field. Two different linearizations of this type have been compared: (1) MPDATA is linearized with respect to both the true wind field and the corrective wind field used in the original transport model algorithm; (2) MPDATA is used with only the true wind field, neglecting the corrective wind field (the donor cell advective algorithm). Both these linearizations produce similar smooth solutions. We choose to use the donor cell advection approximation for the adjoint analysis because it is computationally less expensive. An example of the donor cell adjoint model solution is shown in Figure 1b.

Unlike the transport operators, the free parameters α are always used in the model in, at least, second-order nonlinear products with the concentrations (i.e., products of the form $\chi \alpha$). In the tangent linear model this relationship is linearized as H_α . The adjoint analysis for the free parameters is the linear approximation of the true sensitivity with respect to these parameters, and is valid in the range of small parameter variations. H_α is obtained from the forward numerical integration of HANK.

In solving for the adjoint function χ^* the linear derivative operators H_α and H_χ are updated every 3 hours from the basic state model solution. For intermittent fields, such as the convective mass flux (or rainout), the associated operator is zero for those grid points with no convection (or rainout). Consequently, the adjoint sensitivity $H_\alpha \chi^*$ is exactly zero. In contrast, the adjoint sensitivity to modeled fields which are not intermittent (e.g., model emissions) is evaluated at all grid-points, regardless of the value of the modeled field at that particular location (e.g., for emissions, it is evaluated whether or not emissions are actually present).

4. Model Simulation and Sensitivity Experiments

As discussed by Hess et al. (submitted manuscript, 1999), the time period between April 4, 1992, and May 15, 1992, is simulated with HANK using input fields from the MM5. This period covers the MLOPEX 2c intensive and includes a 10 day model spin-up. Every 2 days the MM5 is reinitialized to prevent excessive model drift (see Hess et al., submitted manuscript, 1999). The corresponding simulated meteorology has a high correlation with the analyzed meteorology, and the simulated deep convection shows a good correspondence with International Satellite Cloud Climatology Project (ISCCP) cloudiness (Hess et al., submitted manuscript, 1999). An independent verification of the model, and in particular a validation of the emissions, transport, and boundary conditions, is achieved by comparing the simulation with chemical measurements made during MLOPEX 2c (Hess et al., submitted manuscript, 1999). The model reproduces many of the measured features and simulates the mean concentrations of most species in agreement with the observations.

The meteorology and trajectories for the examined period are discussed in detail by Hess et al. [1996]. During the MLOPEX 2c period, Hawaii is located, on average, on the eastern edge of the 700 mbar subtropical anticyclone. Hawaii is influenced both by the subtropical anticyclone and the strong westerlies located on average just to the north of the island. Numerous cyclones traverse the Pacific north of Hawaii. Rapid

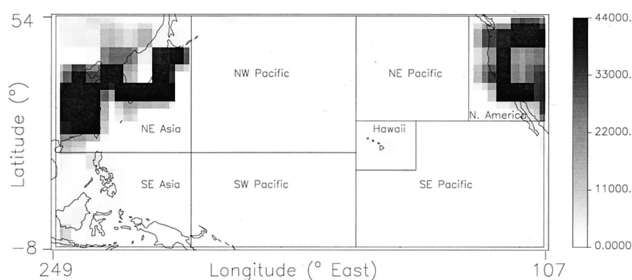


Figure 2. NO_x emissions in HANK in molecules $\text{m}^{-2} \text{s}^{-1}$. The domain in this figure is split into eight regions for model analysis.

fluctuations are observed in the flow regime, with isentropic trajectories to MLO from the east or from the west, as the location of the Pacific anticyclone changes [Hess *et al.*, 1996]. A large fraction of the trajectories are from the northwest Pacific, however, and are characterized by strong subsident motion.

In association with Hess *et al.* (submitted manuscript, 1999), and the MLOPEX 2c experiment, this study examines transport to Hawaii. Two inert trace species are used to study the relevant tropospheric transport pathways: a soluble, but chemically inert species with the same surface emissions as NO (NOYI_s), and a similar, but insoluble species (NOYI_i). In the atmosphere, emitted NO is rapidly transformed into other species in the NO_y family. Two species are used so as to account for the wide range of solubilities of the compounds comprising NO_y . The effective Henry's law solubility of NOYI_i is set to 10^{-36} , while NOYI_s is set to 10^{14} (approximating the solubility of HNO_3). The surface emissions of NO include both anthropogenic and biogenic emissions (Figure 2) (see Hess *et al.*, submitted manuscript, 1999). The emissions maximize over Japan, southern China, and the west coast of North America. As we wish to examine the export of emissions on the Pacific rim to Hawaii, NOYI_i and NOYI_s are not transported into the model from the lateral boundaries. The deposition velocities for both species are taken as the average of the NO and NO_2 deposition velocities.

Above the boundary layer, transport from Asia tends to occur in chemical plumes, often with small vertical dimensions and large horizontal dimensions. Distinct transport events contribute significantly to the average concentration of NOYI_i . Here we concentrate on these transport events. A total of eight experiments were run (Table 2). In the first six of these experiments the instantaneous model sensitivities are examined for both NOYI_i and NOYI_s at a target position x_0 and time τ_2 . The selected target positions are the 900, 680, and 300 mbar pressure levels over Hawaii. The 680 mbar level is selected as the height corresponding to MLO. The target times were selected as the time of the concentration maximum of NOYI_i at each position (see Table 2 and Figure 3). In the experiments described above, the adjoint model is integrated for 2 weeks prior to the target time. Recall that this integration proceeds backward in time. In the final two experiments the sensitivity is computed with respect to the average mixing ratio of both NOYI_i and NOYI_s at 680 mbar for the entire MLOPEX 2c period (April 15 to May 15). In these latter experiments the adjoint integration ends on April 4. In all experiments the sensitivity is computed for an eight point linear interpolation of the model data to the target location.

The time series of NOYI_i and NOYI_s are shown in Figure 3

at each of the target levels, as determined from the basic state model integration. The NOYI_s distribution is multiplied by a factor of 10 in Figure 3, and is only shown for the 2 week period prior to the target time. The fact that NOYI_s is so much smaller than NOYI_i suggests that rainout is extremely important in determining the transport of highly soluble species to Hawaii.

The plume at 300 mbar which we have selected to examine can be traced to a convective event. Convection occurs over southern Asia approximately 4 days prior to when the plume reaches Hawaii (see Figure 4). Hess *et al.* (submitted manuscript, 1999) show that convection was observed in the same area from satellite data. Once convectively lofted, the NOYI_i is rapidly transported in the upper troposphere to Hawaii. The tracer plume at 680 mbar can be traced to a synoptic system which passed over Asia approximately 5 days earlier. The emissions are initially advected eastward behind a cold front which sweeps across Asia. Subsequently, the associated cyclone amplifies off the coast of Japan, transporting the NOYI northward and upward into the free troposphere. The plume of NOYI_i is then advected nearly isentropically to the 680 mbar level at Hawaii. Hess *et al.* (submitted manuscript, 1999) indicates that both of these transport events can be detected in the aircraft chemical measurements documented by Ridley *et al.* [1997]. The effect of local emissions is a significant contributor to the event examined at 900 mbar. However, an anticyclone amplifying over the eastern Pacific also contributes to this event. This weather system is able to tap the high levels of NOYI on the west coast of North America and transport them to Hawaii within the boundary layer.

5. Interpretation of the Adjoint Solution

Using the adjoint model, we compute the sensitivity of NOYI at the target points and times to model parameters and to the initial and boundary conditions. In each case the adjoint model is subject to the appropriate forcing (equation (8)). Note that the measured solution sensitivity ΔJ is equivalent to the change in the species concentration ($\Delta\chi(x_0, \tau_2)$) at the target position x_0 and selected verification time τ_2 in the instantaneous experiments. Specifically,

$$\Delta\chi(x_0, \tau_2) = \sum_m \sum_i \sum_n \chi_i^{*n} (H_{\alpha_m}) \Delta\alpha_{mi}^n + \sum_i \chi_i^{*n} \Delta\chi_i^n + \sum_n \sum_j \chi_j^{*n} \Delta\chi_j^n \quad (11)$$

for lag times $t_n < \tau_2$. Equation (11) gives the change of χ at

Table 2. Experiments Run With the Adjoint Model

Experiment	Species	Verification Point	
		Pressure, mbar	Date
E900 _i	NOYI_i	900	May 2, 0000 UT
E900 _s	NOYI_s	900	May 2, 0000 UT
E680 _i	NOYI_i	680	April 26, 1200 UT
E680 _s	NOYI_s	680	April 26, 1200 UT
E300 _i	NOYI_i	300	May 3, 1200 UT
E300 _s	NOYI_s	300	May 3, 1200 UT
E[680 _i]	NOYI_i	680	April 5, 0000 UT to May 14, 1200 UT
E[680 _s]	NOYI_i	680	April 5, 0000 UT to May 14, 1200 UT

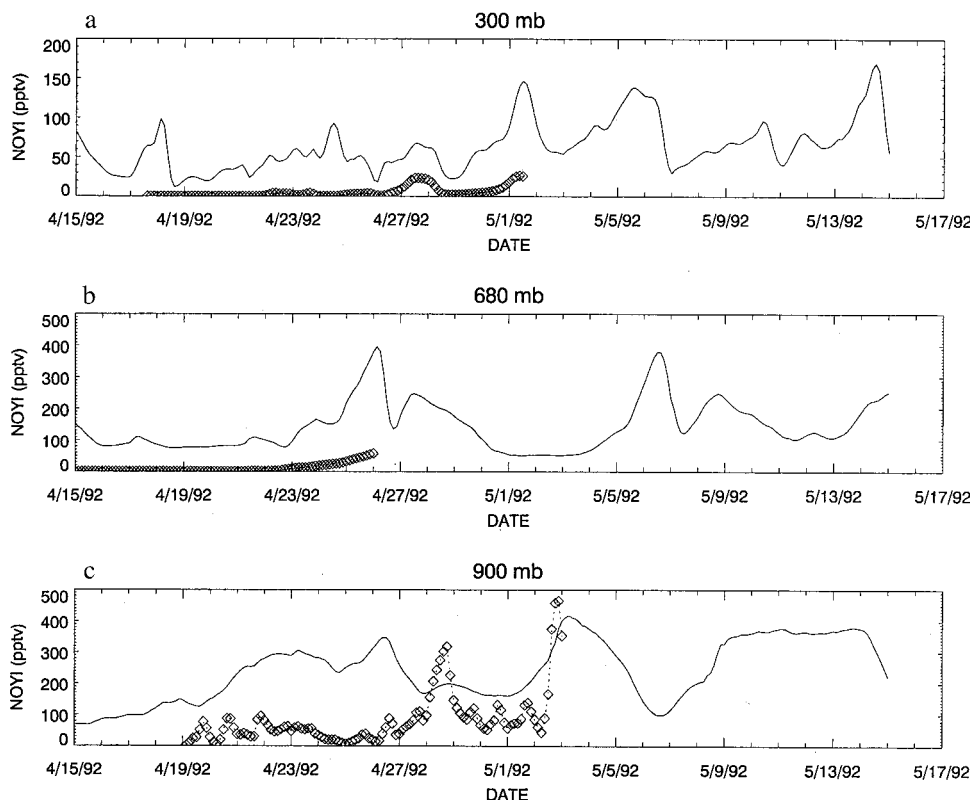


Figure 3. Time evolution of NOYI (pptv) at MLO: (a) 300 mbar, (b) 680 mbar, and (c) 900 mbar. The mixing ratio of the soluble species NOYI_s (diamonds) is multiplied by a factor of 10.

the MLO evaluated using discrete operators, where n is the temporal index, i is the spatial index, j is the boundary index, and m is the parameter index. Each entry in (11) gives an independent contribution to $\Delta\chi(x_0, \tau_2)$ and has been discussed in relation to (9). When evaluating the sensitivity of the time-averaged solution $[\chi]$, the left-hand side of (11) should be replaced by $[\Delta\chi(x_0)]$.

The perturbations in (11) ($\Delta\alpha_{mi}^n$, $\Delta\chi_i^n$ or $\Delta\chi_j^n$) are in general arbitrary. To compare the influence of a controlling parameter in different locations, or to compare the influence of different parameters, we normalize these perturbations. Dif-

ferent normalizations have different interpretations. We choose to examine two different normalizations.

The first normalization examines the percentage change in $\chi(x_0, \tau_2)$ to a percentage change in the controlling parameter. That is, given a perturbation in the parameter α of $0.01 \times \alpha_{mi}^n$, we want to find the percentage change in the mixing ratio at the target point: $\Delta\chi(x_0, \tau_2)/(0.01 \times \chi(x_0, \tau_2))$. We get the desired result taking the parameter perturbation as

$$\Delta\alpha_{mi}^n = \alpha_{mi}^n / \chi(x_0, \tau_2).$$

The form of the perturbation in the mixing ratio is exactly analogous:

$$\Delta\chi(x, t) = \chi_i^n / \chi(x_0, \tau_2)$$

where $\chi(x_0, \tau_2)$ is obtained using the donor cell advection algorithm in the HANK. For consistency, the adjoint solutions are normalized with the mixing ratios in the target region that are computed using the donor cell approximation. This normalization gives the “relative sensitivity” to the controlling parameters, as the adjoint solution χ_i^{*n} is multiplied (weighted) with the actual parameter value (i.e., α_{mi}^n) or mixing ratio (i.e., χ_i^n). The resulting perturbation is spatially dependent, a function of the parameter or mixing ratio at domain gridpoint i or boundary gridpoint j . For example, if χ is zero at the model boundaries, or the emissions are zero, the relative sensitivity to a change in the boundary conditions or emissions is identically zero.

In the second normalization the perturbation for each controlling parameter (or mixing ratio) is normalized with a constant amplitude throughout the domain, regardless of the ac-

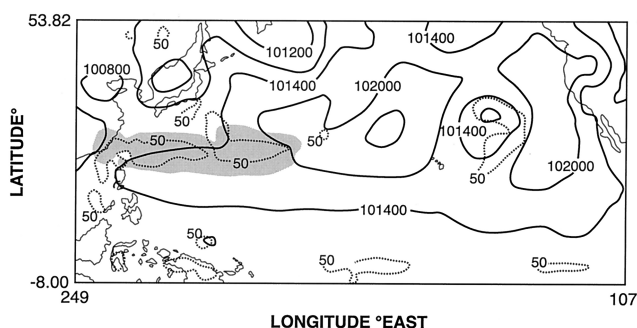


Figure 4. Relative sensitivity (shaded at 10% of maximum sensitivity) of NOYI_i for E300 to perturbations in the NOYI mixing ratio, superimposed on the actual convective mass flux ($\text{kg m}^{-2} \text{s}^{-1}$, scaled by 10^4) (light contours) and the sea level pressure (pascals) (heavy contours). This figure views the three-dimensional relative sensitivity isosurface from top down, projecting it onto the horizontal plane.

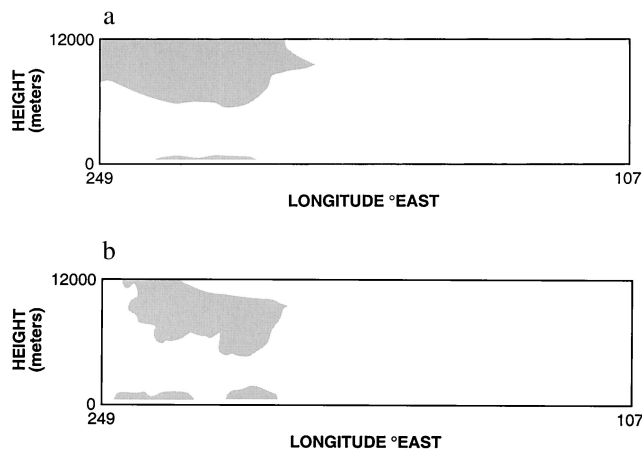


Figure 5. Vertical cross section of (a) absolute and (b) relative sensitivity to perturbations in the NOYI mixing ratio over the most sensitive region in Figure 4. Areas are shaded at 10% of maximum sensitivity. This figure views the three-dimensional relative sensitivity isosurface looking to the north.

tual amplitude of the parameter at a particular position and time. Here we normalize the perturbation using the temporal and spatial average of the controlling parameter $[\bar{\alpha}_m]$ or mixing ratio $[\bar{\chi}]$. This normalization gives the percentage change in mixing ratio at the target point due to a percentage change in the average controlling parameter or mixing ratio. Note that the resulting perturbation does not depend on the model grid point. It takes the form

$$\Delta \alpha_{mi}^n = [\bar{\alpha}_m] / \chi(x_0, \tau_2).$$

A similar expression holds for the perturbation mixing ratio $\Delta \chi$. This result is referred to as the “absolute” sensitivity. Even in locations where emissions are zero, the absolute sensitivity to emissions may not be zero. Therefore the absolute sensitivity gives the potential sensitivity to emissions. However, recall that for intermittent processes, the derivative operators are identically zero in locations where the process is not occurring in HANK. Ideally, to evaluate the impact of potential errors in the parameters on the transport model solution, the error estimates should have been used in weighting the adjoint solution instead of the basic state. Reliable error estimates are, however, virtually impossible to obtain for most parameters.

The adjoint solution can be used to evaluate the sensitivity of NOYI at the target position to the distribution of NOYI at prior times t_n . The sensitivity is simply given by $\chi^*(x, t_n) \Delta \chi(x, t_n)$. Either the absolute sensitivity or the relative sensitivity can be used. In either case the associated region of solution sensitivity can be used to determine where an air mass came from, much like a model trajectory. If the atmosphere were nondiffusive, the absolute and relative sensitivities would be numerically different, but would be collocated. Furthermore, discounting the nonlocal transport associated with parameterized convection, they would be nonzero only along the backward trajectory. The implicit numerical diffusion enlarges the region of influence from a single point to a three-dimensional region, the effect of mixing which is not accounted for in a trajectory analysis. Furthermore, the absolute and relative sensitivity analysis give somewhat different regions of influence in a diffusive atmosphere. In an advective regime (i.e., advection dominates) the maximum absolute sensitivity

will be along the backward trajectory. However, the relative sensitivity is weighted by the actual concentration of NOYI and might not maximize along the trajectory.

In the final two experiments we examine the adjoint sensitivity of the time mean concentrations at MLO. This analysis does not examine a particular transport event, but instead examines the average sensitivity to many transport events. In the time average analysis the adjoint solution (at time t_n and position x) gives the cumulative sensitivity to all transport events at x which affect the model solution at the target point x_0 within the time interval (t_n, τ_2) , where τ_2 is the end of the averaging period. The associated region of influence can be roughly interpreted in terms of a back trajectory analysis performed for all lag times within interval (t_n, τ_2) . Consequently, the zone of influence in the averaged experiment is much broader than the result for the equivalent instantaneous experiment. The zone of influence for the time average MLO concentration extends over all quadrants from Hawaii (not shown).

6. Results

In this section we discuss results for the instantaneous and average sensitivity experiments for both the soluble and non-soluble NOYI species.

6.1. Example of the Adjoint Solution

An example of the relative and absolute sensitivity to NOYI, prior to the target time is shown in Figures 4 and 5. Figure 4 shows the surface pressure, the convective mass flux, and a horizontal projection of the relative sensitivity approximately 4 days prior to when the plume of elevated NOYI reaches the target point of 300 mbar over Hawaii. The convective event occurs in the western Pacific primarily over the ocean in the vicinity of a trough in surface pressure. At this time the convective mass flux and the adjoint sensitivity are almost exactly collocated in latitude and longitude. Figures 5b and 5a show a side view of the relative and absolute sensitivities 6 hours later. The relative sensitivity is large both at the surface and in the upper troposphere. This indicates that in both these locations NOYI is already nonzero and that the solution is sensitive to perturbations in NOYI. The sensitivity in the upper troposphere is due to NOYI which has previously been convectively lofted from the boundary layer. The sensitivity at the surface is due to air which has not yet been convectively lofted, but will be lofted in the immediate future. Figure 5a shows the absolute sensitivity at the same time. The absolute sensitivity does not exactly coincide with the relative sensitivity, but is expanded in volume. Importantly, it extends to the model boundaries, indicating model inflow which could potentially influence the target point. NOYI is explicitly set to zero at the model boundaries, however. Therefore the air flowing into the model contains no NOYI, and acts to dilute the NOYI brought up from the surface in the convective plume.

Figures 4 and 5 demonstrate the strengths of the adjoint technique for analyzing parcel history. As opposed to trajectory analysis, the adjoint analysis accounts for the effect of the entire transport model transfer function. It indicates how transport actually influences the model solution. The sensitivity to parameterized convection is convincingly captured in Figure 4, but would not be captured by a trajectory analysis. Figures 4 and 5 also show the important effect of atmospheric dilution, which spreads the solution sensitivity over a considerable vol-

ume. Calculations of the photochemical age of air, as determined by measured hydrocarbon ratios, indicate the importance of dilution [McKeen *et al.*, 1990].

6.2. Sensitivity to Emissions

The absolute and relative sensitivity of average NOYI_i at 680 mbar ($E[680]_i$) to emissions is shown in Figure 6. The map of absolute sensitivity shows all locations where NOYI_i could have been transported from the model lower boundary to MLO within the 4 week period, given a fixed emission perturbation set everywhere to 1% of the average emissions within the domain. Convoluting the absolute sensitivity with the actual emissions, and dividing by the fixed emission perturbation, gives the relative emission sensitivity (Figure 6b). Figure 6b gives the locations where both the emissions are nonzero and where transport was actually to MLO. At each location the figure gives the percentage increase in average NOYI_i at MLO due to a percentage increase in the emissions at that location.

The magnitude of absolute and relative sensitivities cannot be strictly compared due to their different normalizations. The geographic position of the two sensitivities is markedly different, however. The area of absolute emission influence is much larger than the area of actual influence, as it includes many regions with no actual emissions. Potential emissions in Southeast Asia and immediately offshore in the Pacific could have the most influence on the concentration of NOYI_i at 680 mbar over Hawaii. The actual emissions which affect Hawaii are primarily concentrated over a small region of southern Japan and China during this time period. Emissions from North America, interior China, and northern Japan have relatively little influence at Hawaii. The absolute emission sensitivity can be used to investigate the impact of different scenarios of emission distribution. In a similar manner, adjoint model solutions have been used in inverse modeling studies to evaluate potential sources and sinks of atmospheric CO_2 [see Kaminski *et al.*, 1999a, b, and references therein]. It is not the purpose of this study to investigate this in detail, however. Here we only

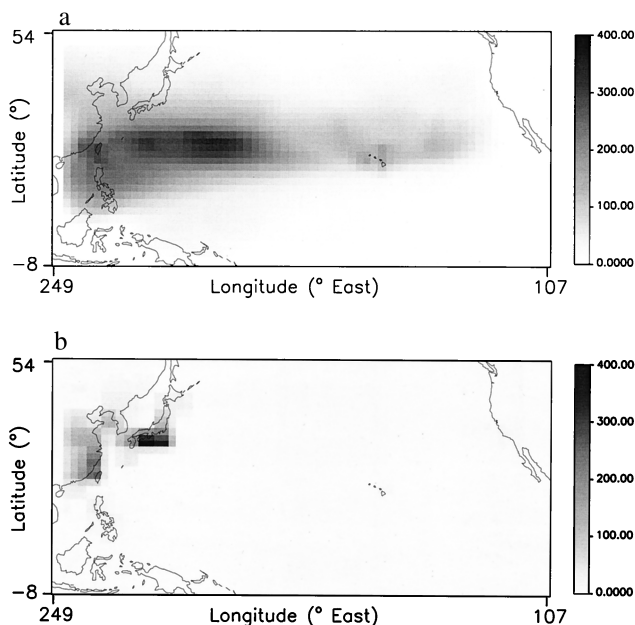


Figure 6. (a) Absolute and (b) relative sensitivity to emissions in $E[680]$. Plotted values are multiplied by 10^5 .

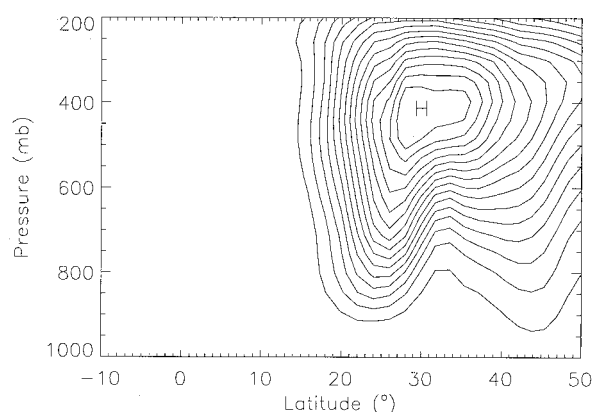


Figure 7. Absolute sensitivity to the western boundary influx. Contour interval is $3 \times 10^{-6}\%$.

examine a single month of springtime transport, which is not sufficient to draw reliable conclusions on the impact of unconsidered, or future emission distributions at MLO.

6.3. Sensitivity to Lateral Boundary Conditions

The lateral boundary conditions are also important to the simulation. In the current model configuration inflow from the lateral boundaries simply dilutes the concentration of the modeled emissions. In reality, the measured chemical concentrations at MLO can be attributed to both emissions from within the considered model domain, and emissions upwind. Figure 7 shows the absolute sensitivity of the average mixing ratio at MLO ($E[680]_i$) to a fixed perturbation in NOYI_i on the western boundary. The absolute sensitivity peaks near 400 mbar over northeast Asia. This shows the importance of air from the upper troposphere on the concentrations at MLO. Trajectory calculations [Hess *et al.*, 1996] show the majority of trajectories descending from the northwest. Below approximately 550 mbar the absolute sensitivity at the western boundary has a double-peaked structure.

6.4. Emission Influence Distributions

The amount of NOYI which is emitted from any point and which eventually reaches Hawaii is time-dependent, depending on the meteorology and the associated transport. The emissions in HANK do not vary in time. Therefore the amplitude of the transfer function at time t is a measure of the importance of the transport pathway at that particular time to Hawaii. The influence of emissions on $\chi(x_0, \tau_2)$ from any grid point can be quantified in terms of an emission influence distribution (EID). This distribution simply consists of the relative (or absolute) emission sensitivity at that point as a function of time.

As the adjoint is linear, the net influence of a region on Hawaii is simply equal to the sum of the influence of the individual grid points (expression (11) in section 5). Summing the EID over all grid points in a particular region gives a regional distribution, a measurement of the transport characteristics over that particular region. For this purpose, the model domain is divided into eight distinct regions. The EID, presented in terms of the relative sensitivity over the regions with significant emissions, is presented in Figure 8 for each experiment. In a diffusive atmosphere, emissions from many regions can simultaneously influence the modeled concentration at a particular position and time. This can occur as the

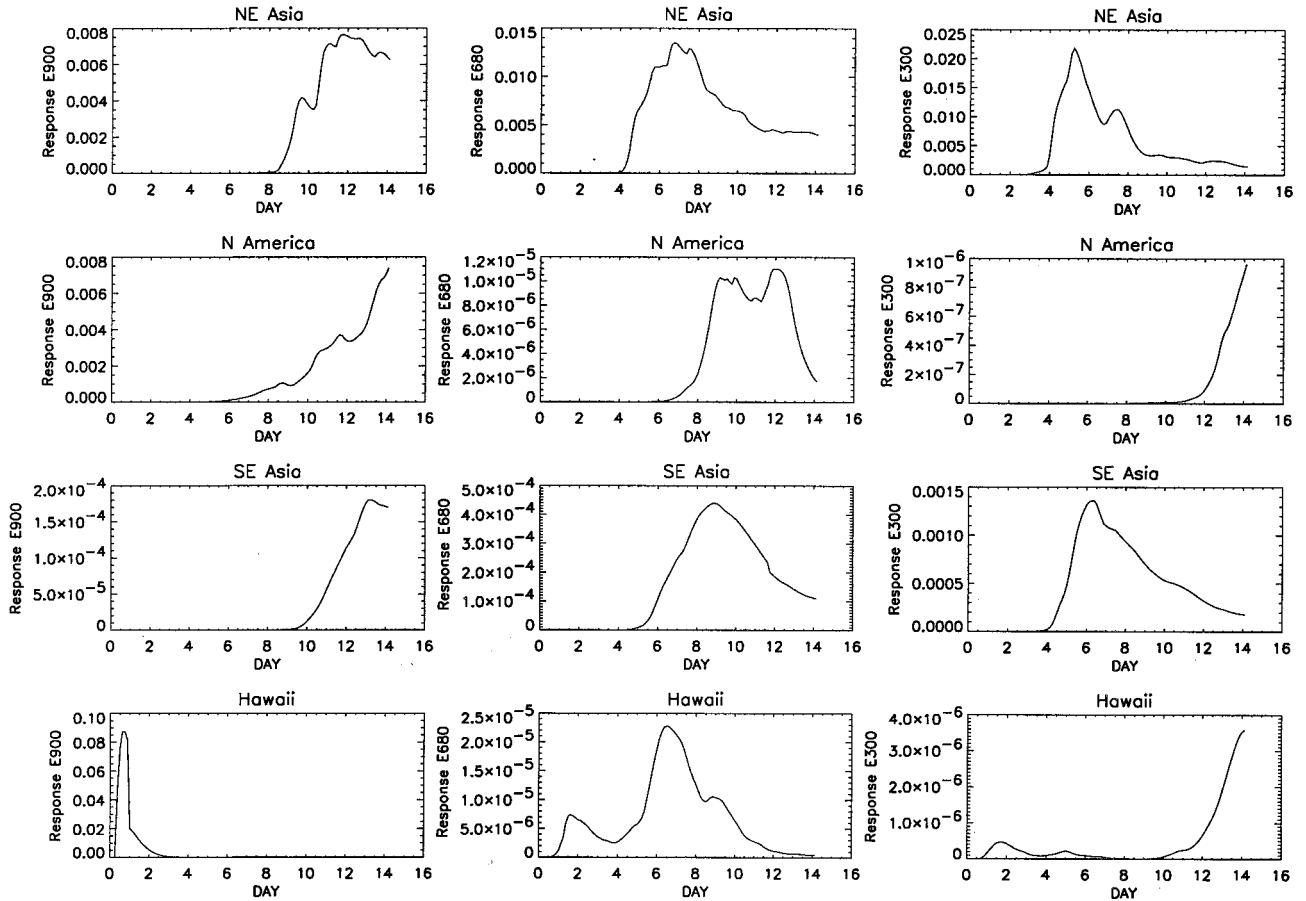


Figure 8. Relative emission influence spectra for different domains and experiments (percent response to 1% change in emissions). The experiments are described in Table 2.

main tracer plume mixes with the background atmosphere, an atmosphere influenced by emissions from all sectors.

The EID can be characterized in terms of its amplitude and its shape. The peak amplitude gives the maximum influence of any region; the average amplitude is a measure of the average influence (see section 6.6, for example). The shape of the EID can be characterized by three timescales: (1) time when the sensitivity is first significant (T_f), measured as the time the signal amplitude first reaches 10% of its maximum amplitude; (2) time when the sensitivity is maximum (T_{\max}) and (3) time of average influence, computed as

$$T_{\text{aver}} = \frac{\sum t_n (\chi_n^* H_\alpha \Delta \alpha)}{\sum (\chi_n^* H_\alpha \Delta \alpha)}$$

where the summation is performed over time index n . T_f characterizes the time of first influence, a measure of the fastest transport time between an emission region and Hawaii; T_{\max} represents the time at which the highest amplitude transport event occurs over the 2 week integration period; T_{aver} gives the average time for transport from a particular region to Hawaii. These times are independent of the actual emission amplitude and are simply the consequence of transport for a given period. These three timescales are shown graphically in Figure 9.

The plume of NOYI_i examined at 300 mbar (E300_i), is primarily influenced by NE Asian emissions, with a transport time of approximately 5 days to Hawaii (see Figures 8 and 9).

The plume is reinforced by emissions from SE Asia with a transport time of 6 days to Hawaii. The difference between the time of maximum influence (T_{\max}) and the time of first influence (T_f) is approximately a day in each case. This time difference is partially attributable to length of the event which vents the boundary layer and partially to diffusion and differential advection within the plume as it travels eastward toward Hawaii. The average time for emissions over NE and SE Asia to influence Hawaii at 300 mbar during this period is approximately 7 and 8 days, respectively. The local influence from Hawaii and the influence from North America is relatively insignificant at 300 mbar. Furthermore, it takes a long time for the signal from these emission regions to propagate to 300 mbar over Hawaii.

At 680 mbar (E680) the maximum amplitude of the NE Asia EID is several orders of magnitude larger than the distribution from the other regions. This is consistent with the relative sensitivity map (Figure 6b). The shape of the NE and SE Asian EID is similar to that at 300 mbar, except the width is wider. The local EID from Hawaii and the EID from North America have two peaks, indicating that two separate transport events influence the solution from each region. In the Hawaiian case, for example, emissions 2 days and 6.5 days prior to the target time influence the concentration at 680 mbar over Hawaii. The peak influence of SE Asian emissions at 680 mbar is an order of magnitude less than at 300 mbar, while the influence of Hawaii and North America is approximately an order of mag-

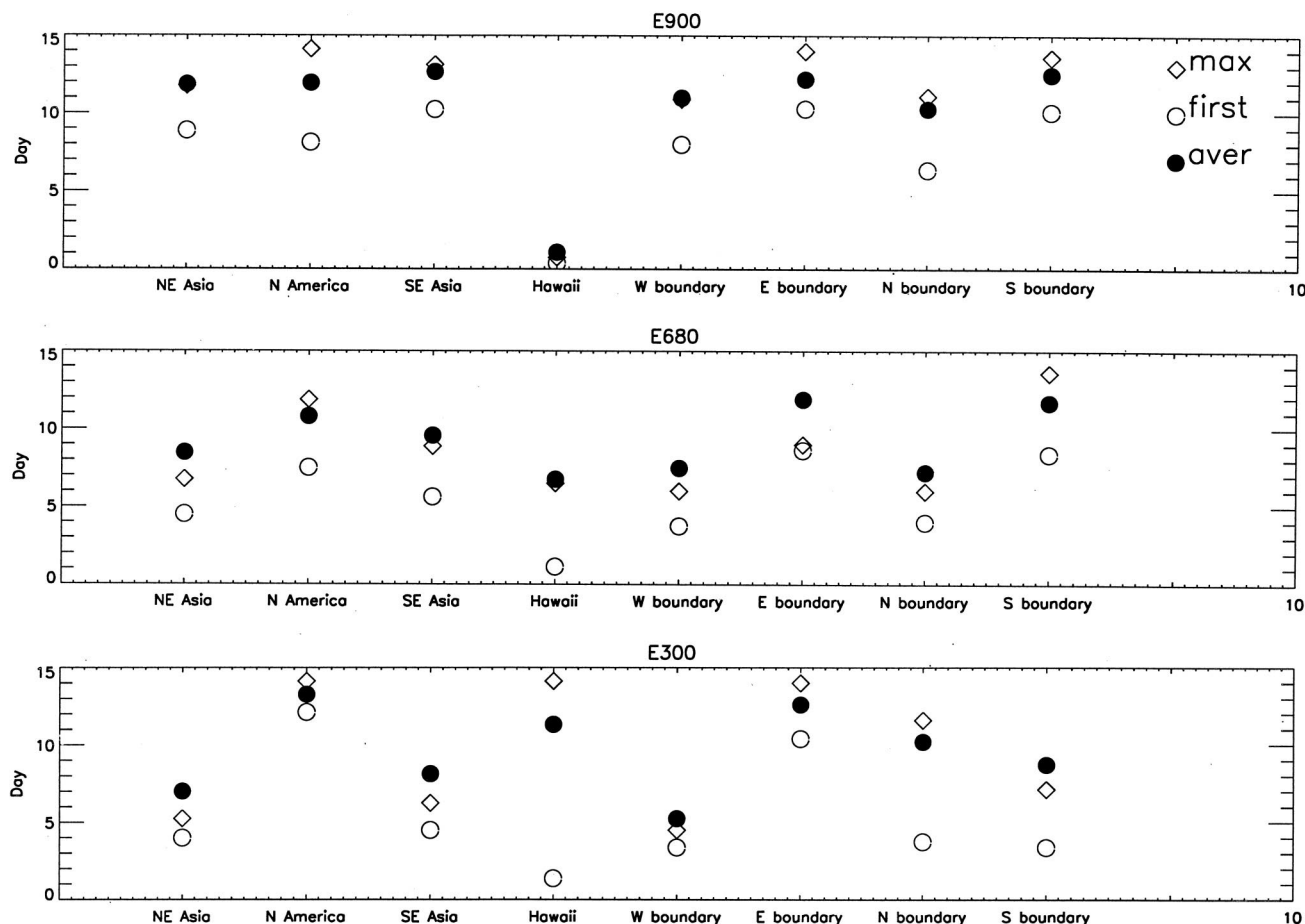


Figure 9. Characteristic emission influence times (days) for different regions and different experiments, including the lateral boundaries. The experiments are described in Table 2.

nitude larger. The travel times from NE and SE Asia are longer at 680 mbar than at 300 mbar due to the slower westerly winds at the lower levels. However, the travel times from America and Hawaii are faster due to the greater proximity to the boundary layer.

The EID at 900 mbar (E900,) show very different characteristics than those in the free troposphere. First, the regions of influence and the travel times are different at 900 mbar. Local emissions have a pronounced and almost immediate effect on the solution, while on longer timescales (greater than 10 days), Asian and North American emissions influence the concentrations at Hawaii. Second, the distribution width is considerably broader at 900 mbar than at the upper levels, indicating a more diffuse signal. This can be attributed to the long transport timescales and the high boundary layer diffusivity.

6.5. Boundary Influence Distributions

Influence distribution can also be computed at the lateral boundaries through a summation of the individual response distributions at each point along the boundary. These distributions are shown in Figure 10. The associated timescales are given in Figure 9. It is necessary to use the absolute sensitivity to compute the boundary response. The zero inflow boundary condition imposed on NOYI forces the relative sensitivity to be exactly zero at the model boundaries. At all levels the potential influence of the eastern boundary is insignificant, with a relatively minor contribution even in the boundary layer. The in-

fluence distribution for the western boundary shows a pronounced peak in each experiment. This suggests that during the primary transport event the emitted species is diluted considerably by inflow from the western boundary. This influence increases with height, consistent with the increase in the westerly winds. At 300 mbar the western boundary is by far the most influential boundary. The stronger winds at the higher levels also decrease the influence time there: T_{\max} is 10 days on the western boundary at 900 mbar and 5 days at 300 mbar. At all levels the western boundary influence distribution resembles the NE Asian EID (Figure 8). The other boundaries tend to show more complex influence distributions, with multiple peaks often found. Influence peaks on the western and northern boundaries are often coincident, suggesting a northwest flow to Hawaii. The influence of the northern lateral boundary decreases with height. At the 900 mbar level both the northern and western boundaries have comparable influence.

Ultimately, any trace species which arrives at MLO has been emitted at the surface, or advected from the model boundaries. Using the adjoint solution, we can estimate the relative importance of Asian emissions at Hawaii compared to upstream emissions advected through the model lateral boundaries. A time integral of the boundary influence distributions gives the net sensitivity along each boundary. The absolute sensitivity response function is also computed at the lowest model level, and integrated over the entire model simulation. In the latter calculation only those points with surface emissions in the

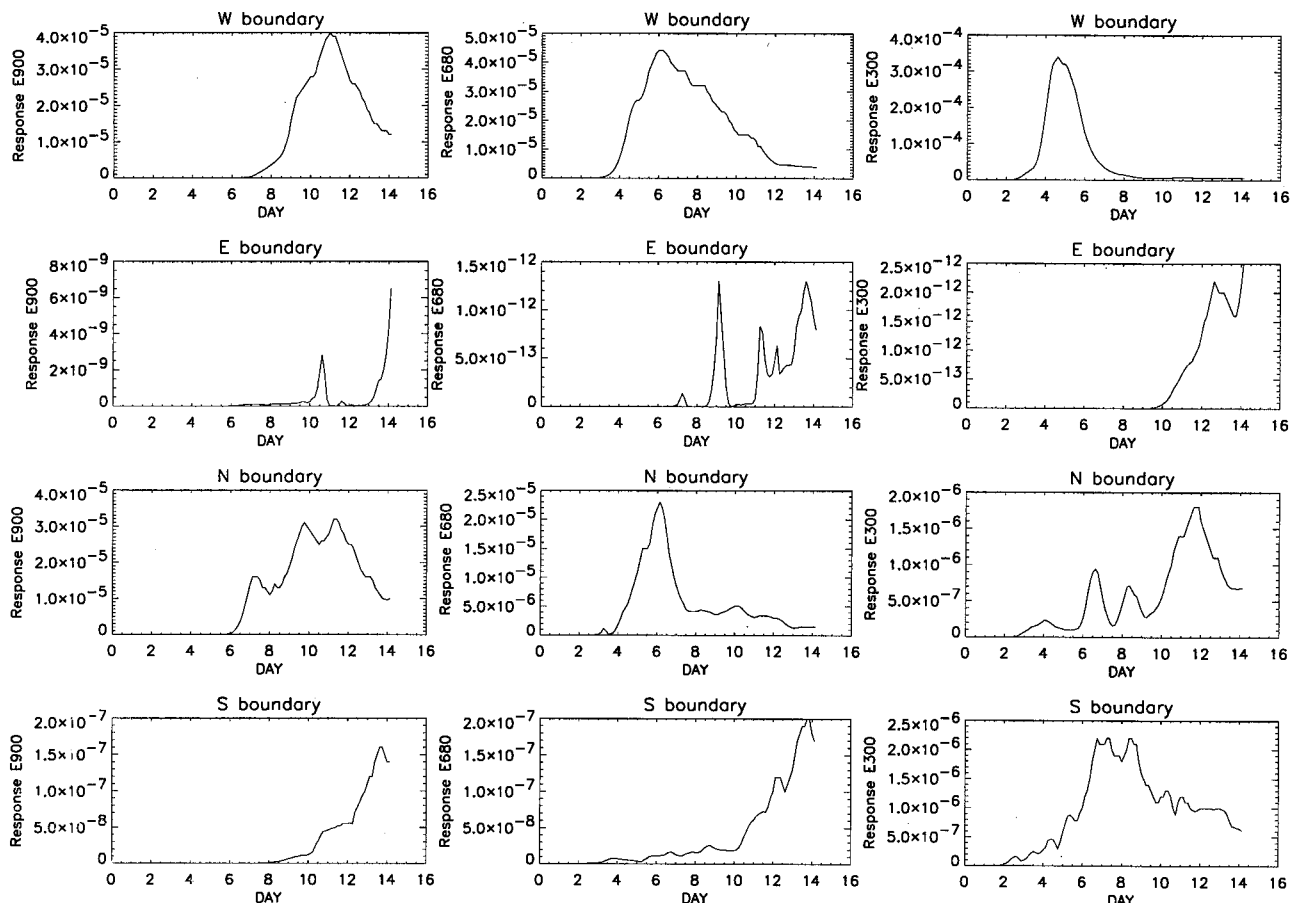


Figure 10. Potential emission influence spectra for different lateral boundaries and experiments. The experiments are described in Table 2.

western portion of the model domain are used. On each boundary we use the sensitivity response to the average mixing ratio at 680 mbar as calculated in $E[680]_i$. These results show that the potential importance of perturbing the mixing ratio of NOYI_i at the surface is a factor of 10 less than perturbing NOYI_i at the northern boundary, a factor of 60 less than a perturbation at the western boundary and comparable to a perturbation at the southern boundary. The influence of the eastern boundary is small. These results are for equal perturbations at the surface and on the boundaries. However, expected perturbations as a result of fluctuations in the wind and concentration of NOYI at the western boundary are not the same as perturbations in the emissions. The largest resolved surface flux of NOYI is approximately $1. \times 10^{15} \text{ molecules m}^{-2} \text{ s}^{-1}$. Therefore a tracer perturbation equal to 1% of these emissions for 1 s is $1. \times 10^{13} \text{ molecules m}^{-2}$. Assuming 200 pptv of NO_y is advected into the model at 500 mbar by a wind of 10 m s^{-1} gives a typical advective boundary flux of $\approx 6 \times 10^{17} \text{ molecules m}^{-2} \text{ s}^{-1}$. A 1% perturbation for 1 s is $\approx 6 \times 10^{15} \text{ m}^{-2}$. Therefore the perturbation induced by emissions is significantly less than that induced through inflow from the western boundary; not only is the solution at Hawaii influenced to a greater extent by the boundary flux than the surface flux, the boundary flux is likely to be much larger.

6.6. Net Sensitivity to Model Parameters

The net sensitivity of NOYI_i and NOYI_s at Hawaii for eight regions and nine model parameters is shown in Figure 11. The

regions are those demarcated in Figure 2 and extend from the surface to the upper model boundary. The parameters and the associated processes are listed in Table 1. The net sensitivity is defined as the time integral of the relative sensitivity distribution of a particular parameter in a particular region. Parameters which govern the redistribution of tracer can have either a positive or negative impact at Hawaii at any time. The parameter perturbation is always assumed to be positive. In Figure 11 the sum over the positive and negative contributions is shown separately. Only four parameters are single signed: the emissions and top boundary condition always have a positive impact at the target point, while dry and wet deposition always have a negative impact. The insoluble species, NOYI_i , is not sensitive to washout in convective (parameter 8) or nonconvective (parameter 9) clouds. Figure 11 also distinguishes the effect of vertical mixing in the boundary layer (PDMC-pbL and NDMC-pbl) from vertical mixing in the free troposphere (PDMC-fa and NDMC-fa). For these purposes the boundary layer is considered to consist of the first six levels (approximately the first 200 mbar). The sensitivity to advection is important, but has not been calculated due to complications in categorizing the response of perturbing a three-dimensional wind field.

Deep convection evokes a particularly complex response. It transports species both upward, in the convective updraft, and downward in the associated large-scale subsident motion and in convective downdrafts. The net sensitivity to deep convec-

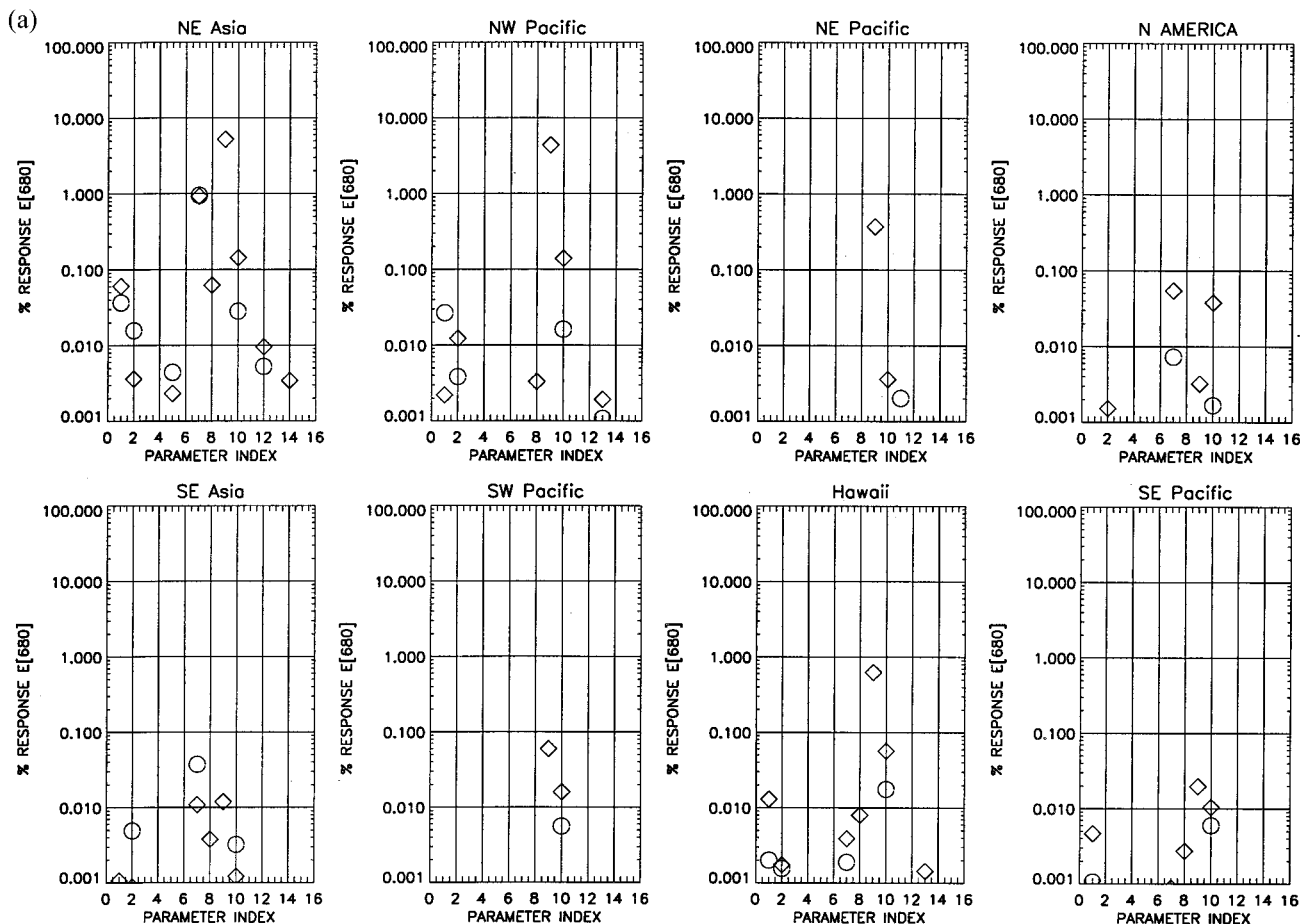


Figure 11. Relative response (in percent) to 1% change in various model parameters in (a) E[680], (b) E680, (c) E300, and (d) E900. The parameters are listed in Table 1. Diamonds are the response for NOYI_s ; circles are the response for NOYI_i .

tion is determined by the sensitivity to the convective mass flux (parameters 1 and 2), and for soluble species, by the sensitivity to the convective rain rate (parameter 8). For NOYI_s (a highly soluble species) the negative sensitivity to the rain rate is often roughly equivalent to the positive sensitivity to the updraft mass flux (Figure 11). Over polluted boundary layers, convection can increase the free tropospheric concentration of emitted soluble species, but decrease the free tropospheric concentration of soluble species. Over clean boundary layers, convection will often reduce the upper tropospheric concentration of both soluble and insoluble species.

In many circumstances the parameter sensitivity is markedly different for NOYI_i and NOYI_s . The discrepancy in sensitivities is accounted for by the factor (see equation (9) and section 5)

$$\left(\frac{\chi(x_0, \tau_2)_i}{\chi(x_0, \tau_2)_s} \right) \left(\frac{(H_{\alpha_m})_s \alpha_m}{(H_{\alpha_m})_i \alpha_m} \right)$$

where m is the parameter index. The ratio of insoluble to soluble species concentrations at Hawaii is large (Figure 3). The ratio of the second term is difficult to predict a priori. H_α measures the linear basic state sensitivity to a parameter change and is a function of the basic state concentrations of NOYI . These are affected by the entire flow history.

6.7. Average Response at 680 mbar

The average mixing ratio at MLO (E[680]) is influenced by all sectors (see Figure 11a). This is in accordance with the trajectory analysis of Hess *et al.* [1996], which shows that within the MLOPEX 2c time frame trajectories approach Hawaii from most sectors. Also consistent with the trajectory analysis is that the largest sensitivities are due to processes over NE Asia, the NW Pacific, and immediately in the vicinity of Hawaii. These regions are within the primary transport pathway which originates from the emissions over NE Asia. The sensitivity to emissions in NE Asia is very close to 1% for both the soluble and insoluble species (parameter 7 in Figure 11a). This is the maximum possible sensitivity to emissions as transport and loss processes are linear in χ . Averaged over all the whole domain, the sensitivity of a 1% increase in emissions is necessarily equal to 1%.

In most sectors the sensitivity response for soluble species is dominated by washout. This response is highly nonlinear. The washout rate is a linear first-order loss for NOYI_s . Therefore increasing the washout rate is equivalent to decreasing NOYI_s exponentially. Figure 11a shows that in the regions along the primary transport pathway to Hawaii (i.e., the NE Asia and the NW Pacific), a 1% increase in the nonconvective rain rate (parameter 9) can decrease the concentration at Hawaii by

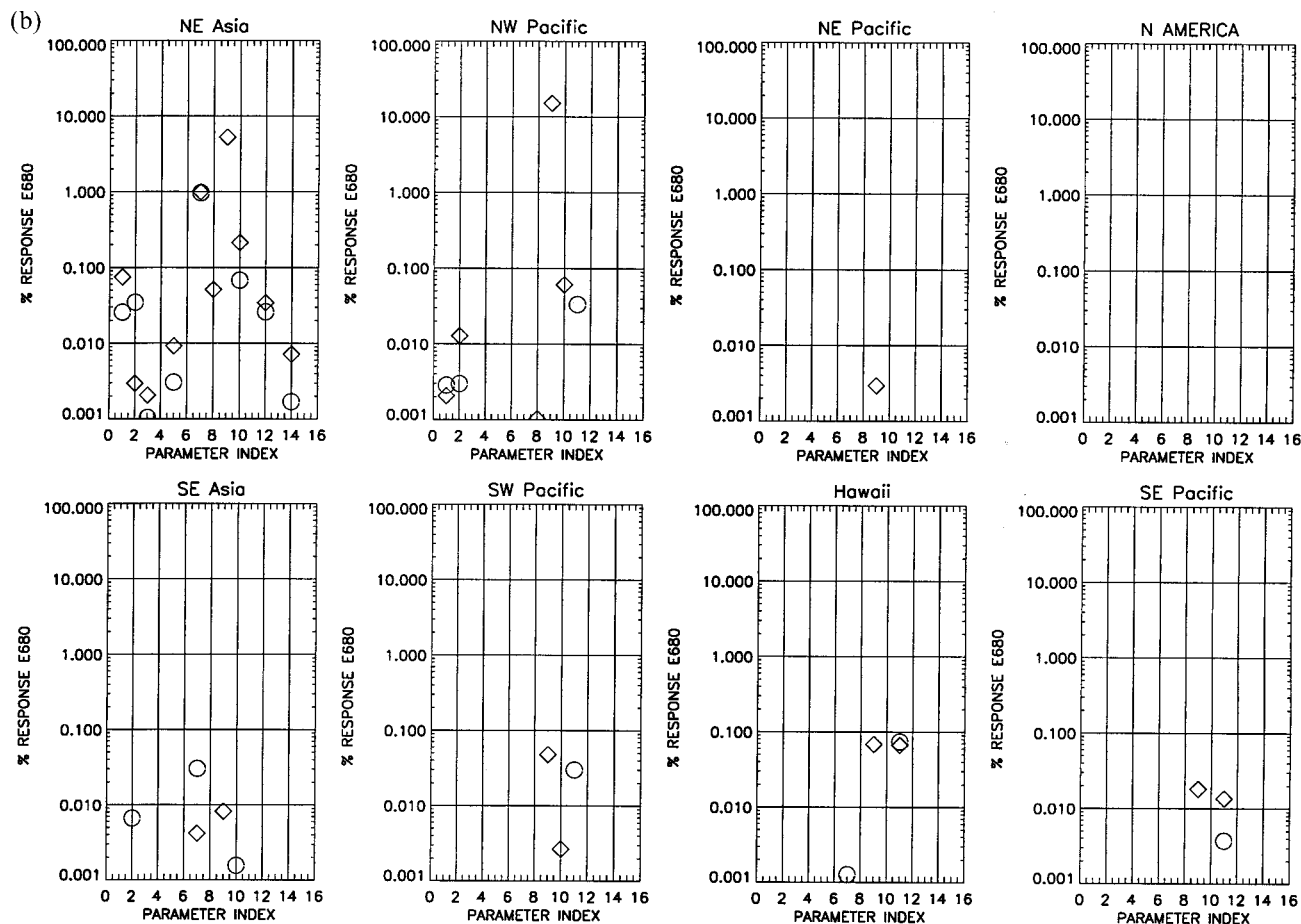


Figure 11. (continued)

almost 6%. Washout by deep convective clouds (parameter 8) is also important in decreasing NOYI_s at Hawaii, but is usually much less influential than the nonconvective washout. In contrast to the large-scale rain events, convection is sporadic and limited in areal coverage.

NOYI emissions must be lofted out of the boundary layer and into the free troposphere to affect the free tropospheric concentrations over Hawaii. However, boundary layer mixing (parameters 12 and 13) generally has a small effect on the simulated NOYI concentration at MLO. Shallow convection (parameters 3 and 4), countergradient mixing (parameters 14 and 15), and dry deposition (parameter 5) are also not important. Only deep convection is moderately important (near the 0.05% level) in venting the boundary layer over NE Asia. Over the NW Pacific the importance of convection is somewhat less, and its sign depends on the species solubility. Both polluted and clean boundary layers are encountered over this ocean sector. We conclude that boundary layer processes are not important in controlling the transport of NOYI to the free troposphere over Hawaii. The transport out of the boundary layer and to Hawaii is controlled by the resolved large-scale winds. As discussed above, it is difficult to compare the sensitivity of parameterized processes with those of resolved large-scale processes.

Free tropospheric mixing is generally more important in regulating the response over Hawaii than convection. This parameter is among the most important model parameter in almost every quadrant, affecting the transport of NOYI after it

is vented out of the boundary layer. On average, vertical mixing tends to increase the concentration of NOYI over MLO.

6.8. Episodic Response at 680 mbar

Recall that the transport to Hawaii in E680 is attributable to a synoptic storm which amplifies off the Asian coast. The episodic sensitivities of NOYI_s and NOYI_t (Figure 11b) are roughly the same as the average response ($E[680]$) over Asia and the NW Pacific. In particular, the sensitivity to emissions over NE Asia is again nearly 1%. However, the sensitivity to shallow convection and boundary layer mixing over NE Asia is somewhat larger in this particular transport episode than in the long-term average. The sensitivities over other regions are generally reduced in comparison to $E[680]$.

6.9. Episodic Response at 300 mbar

The solution at 300 mbar ($E300$) is again most sensitive to processes over NE Asia and the NW Pacific (Figure 11c). Emissions over SE Asia are more important than in the previous cases. The convection responsible for the plume of enhanced NOYI at 300 mbar occurs near the boundary of the NE and SE Asian domains (Figure 4). The convective sensitivities over NE Asia are 10 times larger than those at 680 mbar. The positive convective response (parameter 1), the negative convective response (parameter 2), and the response due to convective rainout (parameter 8) are all enhanced. Vertical diffusion decreases the 300 mbar response at Hawaii, both in the

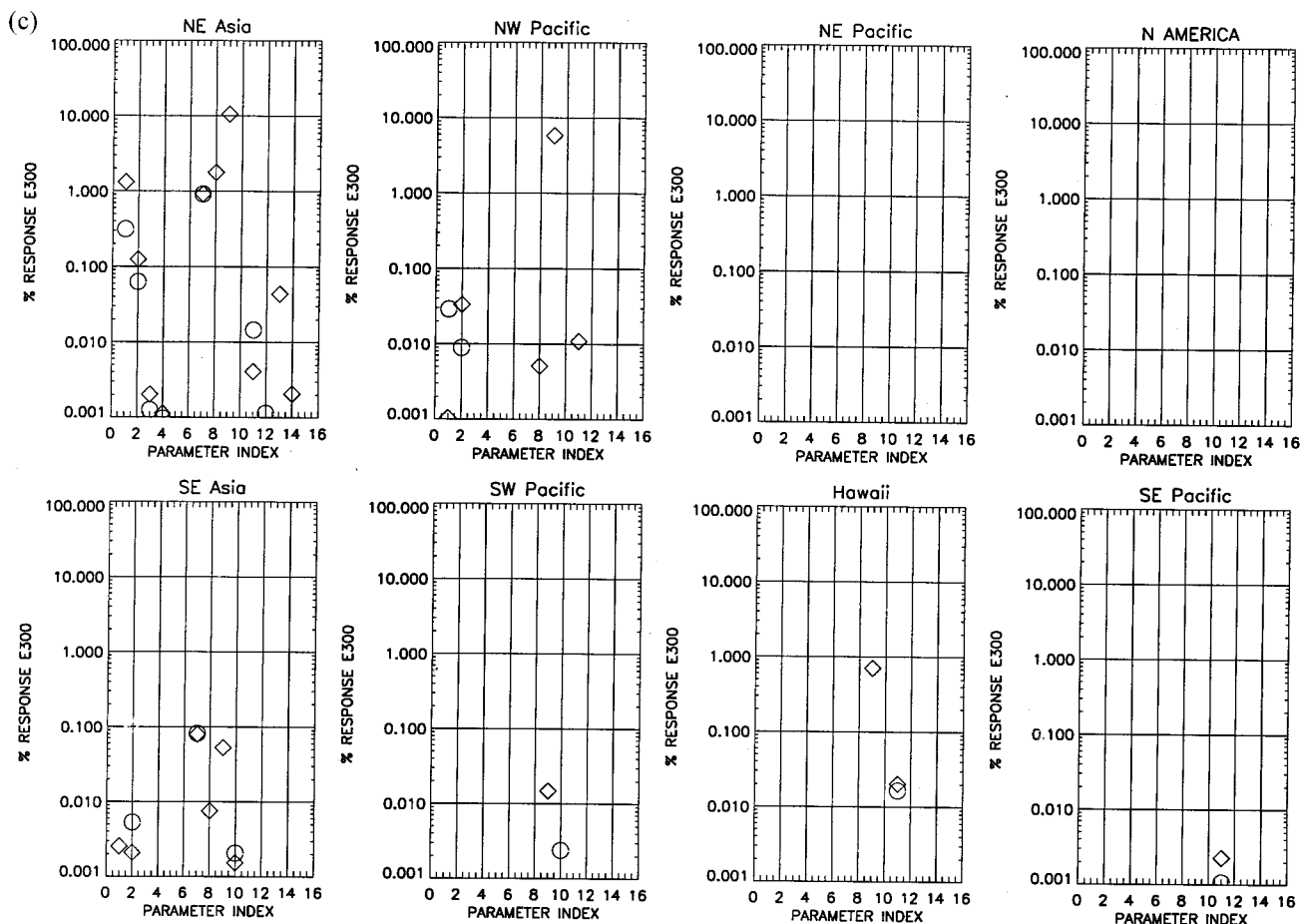


Figure 11. (continued)

boundary layer over NE Asia, and in the free troposphere in a number of the subdomains.

6.10. Episodic Response at 900 mbar

The response at 900 mbar is largely controlled by local processes. The solution is quite sensitive to the local Hawaiian emissions and the local boundary layer transport processes. Boundary layer diffusion and shallow convection decrease the 900 mbar mixing ratio, while the countergradient boundary layer term elicits a modest positive response. Local rainout strongly affects the concentration of the soluble species: a 1% change in the rain rate decreases the concentration of NOYI_s by 10%.

In a diffusive atmosphere the local concentration can be influenced simultaneously through a number of different transport pathways. The 900 mbar solution has a larger sensitivity to a wider variety of emission sources than the other cases examined. Emissions remote from Hawaii are particularly influential for NOYI_s , as it can be transported farther without being washed out. Emissions over North America (in the insoluble case), the SE Pacific, and NE Asia all contribute to the 900 mbar response at approximately the 0.1% level.

Emissions to the east of Hawaii are primarily transported to the island in the boundary layer. Over the SE Pacific the sensitivity to the various transport processes is similar to the local sensitivity: processes which vent the boundary layer induce a negative response. The primary transport pathway from NE Asia is out of the Asian boundary layer, across the Pacific

in the free troposphere, followed by descent into the oceanic boundary layer (not shown). Therefore processes which ventilate the Asian boundary layer evoke a positive response in the boundary layer at Hawaii. The sensitivities to convection, free tropospheric mixing, and boundary layer mixing are all positive over NE Asia. These responses are similar to the free tropospheric responses documented above.

7. Conclusions

In this paper we apply the adjoint technique to diagnose the transport of a chemically inert and insoluble species, and an inert, but soluble species, to Hawaii from emission sources within the greater Pacific Basin. The transport is investigated at times of elevated species mixing ratio in the upper troposphere (300 mbar), the lower free troposphere (680 mbar), and in the boundary layer. In addition, we investigate the average response at 680 mbar. The insoluble species is transported to Hawaii much more readily than the soluble species. This stresses the importance of washout, particularly as species are lofted into the free troposphere, either by convection or large-scale resolved processes. A comparison between HANK and the measurements (Hess et al., submitted manuscript, 1999) does not suggest the washout is excessive.

The adjoint gives the sensitivity of species mixing ratio at a target position and time to the mixing ratio at prior times. Therefore, like a back trajectory analysis, the adjoint technique provides information on a parcel's history. However, as the

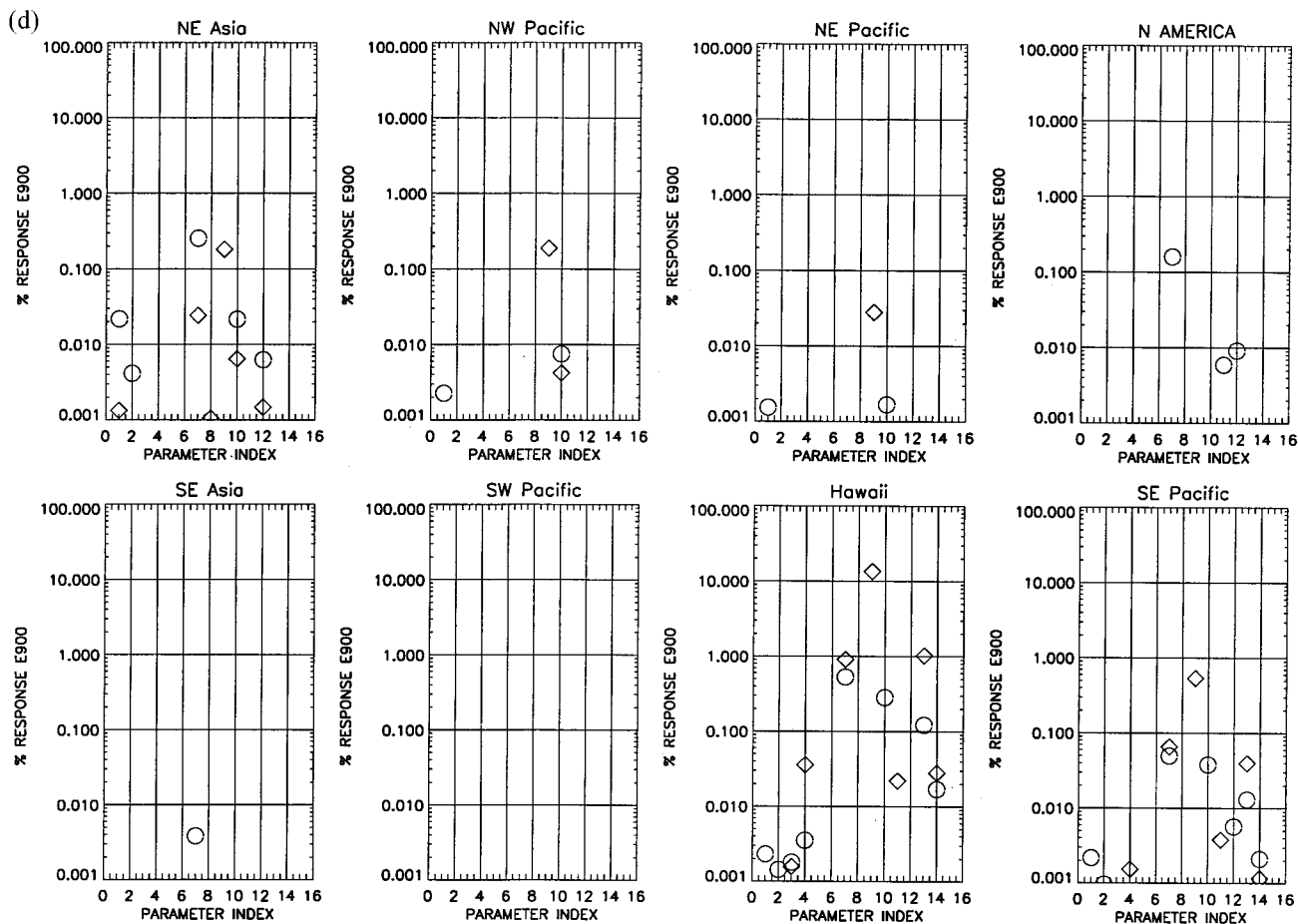


Figure 11. (continued)

adjoint solution includes the effects of implicit diffusion, the region which influences the target point is not a single point as in a trajectory analysis, but is a three-dimensional region. The target point can be simultaneously influenced from different regions by different transport pathways. Conceptually, the associated air parcel is composed of molecules from different locations. This concept is at odds with the idea of an indivisible air parcel traveling along a trajectory from a source region to a target point. It demonstrates the importance of mixing with the background atmosphere. The importance of this mixing has been discussed previously in relation to age of air diagnosed from hydrocarbon ratios within the troposphere [McKeen *et al.*, 1990] and in calculations in a stratospheric context [Hall and Plumb, 1994].

The adjoint analysis includes the effect of transport processes which are not advective, as it includes the entire transport model transfer function. In particular, it includes the effects of boundary layer diffusion, vertical mixing, convection, and wet and dry deposition. Many of these processes are of particular importance in venting the boundary layer of emitted species. Thus, in many ways, the adjoint solution provides the missing link between the emission of pollutants at the surface and their advection through the atmosphere.

The adjoint solution provides a means to compare the relative influence of different processes on the model solution. This allows one to assess the importance of modeling various model processes, but does not determine if the process is parameterized correctly in the first place. As each process in

the model is associated with a set of parameters, the influence of each process is measured in terms of the impact a change in the parameter has on the model solution. Ideally the amplitude of a parameter perturbation should be in accord with its uncertainty. In this case the more highly uncertain parameters would be assigned larger perturbations.

This study shows that for soluble species, the most important process to model accurately is wet deposition by nonconvective rain. The associated response can be highly nonlinear: a 1% change in the rain rate in some regions can decrease the average species mixing ratio at Hawaii by more than 10%. In all instances, wet deposition by deep convection is not as important as nonconvective rain.

Emissions are generally the second most important parameter to model correctly for the soluble species, and the most important parameter for the insoluble species. Overall, a 1% change in emissions everywhere changes the concentration at the target point by 1%. This result should hold in all models, as it depends on the linearity of the transport operators. For inert species (e.g., NO_y), possibly subject to first-order losses, this result can be used in diagnosing whether model error can be attributed to an incorrect estimation of emissions. For example, if the estimated error in modeled NO_y emissions is 50%, and the model meteorology is correct, simulated errors in NO_y greater than 50% cannot be attributed to the model emissions.

Boundary layer transport processes are generally not important in controlling the free tropospheric concentration of NO_y at Hawaii. The sensitivity to shallow convection (param-

eters 3 and 4), countergradient mixing (parameters 14 and 15), and dry deposition (parameter 5) is not large. The venting of the Asian boundary layer, in particular, is not primarily controlled by the parameterized boundary layer mixing. However, boundary layer transport, and the associated boundary layer venting, does sensitively control the concentrations in the boundary layer (i.e., E900). Generally, an increase in boundary layer diffusion, or the shallow convective mass flux, decreases the concentration of NO_YI in the boundary layer.

Deep convection can be important in venting the boundary layer. On average (E[680]), the solution at 680 mbar is somewhat sensitive to deep convection. Higher in the troposphere the importance of deep convection increases. In the episodic 300 mbar case a 1% change in the deep convective mass flux can produce a 1.5% change in the mixing ratio in NO_YI_s at Hawaii. In most of the experiments, and in most of the domains, free tropospheric mixing is more important than deep convection. This process continually acts on a modeled plume as it is advected to Hawaii.

The adjoint analysis clearly shows that during the MLOPEX spring intensive NE Asian emissions have the greatest impact on the free troposphere concentration of NO_YI over Hawaii. However, the solution is potentially more sensitive to inflow through the lateral boundaries than to the considered emissions. This suggests that most of the NO_Y over Hawaii is from upstream of Asia. Although not considered in depth, emissions off the south Japanese coast could have an even larger impact on Hawaii.

The adjoint analysis can also be used investigate individual transport events and the travel time to Hawaii. The 300 and 680 mbar levels at MLO are influenced by regions remote from Hawaii on timescales shorter than 10 days. The western boundary influences the solution in an average of in approximately 5, 8, and 11 days in E300, E680, and E900, respectively. The NE Asian emissions influence Hawaii on average in 9 days at 680 mbar and 7 days at 300 mbar. The fastest transport from NE Asia can occur in approximately 4 days. Transport at 900 mbar from regions remote to Hawaii is slow. The average influence time from North America is 12 days at 900 mbar.

The analysis in this study cannot be trivially performed using standard forward sensitivity techniques due to the large computational burden. The cost of adjoint computations for each diagnostic function is equivalent to the cost of HANK integration. We demonstrate the skill of the adjoint method to efficiently and comprehensively analyze influences of many different processes involved in the transport of chemical species.

Acknowledgments. This research has started while the first author was at the National Center for Atmospheric Research which is sponsored by the National Science Foundation. The first author is currently affiliated with the Corporate Institute for Research in the Atmosphere (CIRA) at the Colorado State University and is funded through DOD's Geosciences project DAAL01-98-2-0078 at CIRA. The second author is affiliated with the NCAR sponsored by the National Science Foundation. Special thanks to L. Smith for helping with graphics and to L. Horowitz and J.-F. Lamarque for thoughtful comments on earlier versions of this manuscript.

References

Anthes, R. A., and T. T. Warner, Development of hydrodynamical models suitable for air pollution and other mesometeorological studies, *Mon. Weather Rev.*, **106**, 1045–1078, 1978.

Atlas, E. L., and B. A. Ridley, The Mauna Loa Observatory Photo-

chemistry Experiment: Introduction, *J. Geophys. Res.*, **101**, 14,531–14,541, 1996.

Davis, D. D., et al., Assessment of ozone photochemistry in the western North Pacific as inferred from PEM-West A observations during the fall 1991, *J. Geophys. Res.*, **101**, 2111–2134, 1996.

Ehhalt, D. H., F. Rohrer, and A. Wahner, Sources and distribution of NO_x in the upper troposphere at northern midlatitudes, *J. Geophys. Res.*, **97**, 3725–3738, 1992.

Giorgi, F., and W. L. Chameides, The rainout parameterization in a photochemical model, *J. Geophys. Res.*, **90**, 7872–7880, 1985.

Godunov, S. K., A difference scheme for numerical computation of discontinuous solutions of equations in fluid dynamics, *Math. Sbornik*, **47**, 271, 1959.

Grell, G. A., Prognostic evaluation of assumptions used by cumulus parameterizations, *Mon. Weather Rev.*, **121**, 764–787, 1993.

Grell, G. A., J. Dudhia, and D. R. Stauffer, A description of the fifth generation Penn State/NCAR Mesoscale Model (MM5), *Tech. Note NCAR/TN-398+LA*, 116 pp., Natl. Cent. for Atmos. Res., Boulder, Colo., 1993.

Hall, M. C. G., D. G. Caccuci, and M. E. Schlesinger, Sensitivity analysis of a radiative convective model by the adjoint method, *J. Atmos. Sci.*, **39**, 2083–2050, 1982.

Hall, T. M., and R. A. Plumb, Age as a diagnostic of stratospheric transport, *J. Geophys. Res.*, **99**, 1059–1070, 1994.

Hecht, M. W., W. R. Holland, and P. J. Rasch, Upwind-weighted advection schemes for ocean tracer transport: An evaluation in a passive tracer context, *J. Geophys. Res.*, **100**, 20,763–20,778, 1995.

Hess, P. G., N. Srimani, and S. J. Flocke, Trajectories and related variations in the chemical composition of air for the Mauna Loa Observatory during 1991 and 1992, *J. Geophys. Res.*, **101**, 14,543–14,568, 1996.

Hoell, J. M., D. D. Davis, S. C. Liu, R. E. Newell, M. Shipman, H. Akimoto, R. J. McNeal, R. J. Bendura, and J. W. Drewry, The Pacific Exploratory Mission-West A (PEM-West A): September–October 1991, *J. Geophys. Res.*, **101**, 1641–1653, 1996.

Hoell, J. M., D. D. Davis, S. C. Liu, R. E. Newell, H. Akimoto, R. J. McNeal, and R. J. Bendura, The Pacific Exploratory Mission-West Phase B: February–March, 1994, *J. Geophys. Res.*, **102**, 28,223–28,239, 1997.

Holtlag, A. A. M., and C.-H. Moeng, Eddy diffusivity and countergradient transport in the convective atmospheric boundary layer, *J. Atmos. Sci.*, **48**, 1690–1698, 1991.

Kaminski, T., R. Giering, and M. Heimann, Sensitivity of the seasonal cycle of CO₂ at remote monitoring stations with respect to seasonal surface exchange fluxes determined with the adjoint of an atmospheric transport model, *Phys. Chem. Earth*, **21**, 457–463, 1996.

Kaminski, T., M. Heimann, and R. Giering, A coarse grid three-dimensional global inverse model of the atmospheric transport, 1, Adjoint model and Jacobian matrix, *J. Geophys. Res.*, **104**, 18,535–18,553, 1999a.

Kaminski, T., M. Heimann, and R. Giering, A coarse grid three-dimensional global inverse model of the atmospheric transport, 2, Inversion of the transport of CO₂ in the 1980s, *J. Geophys. Res.*, **104**, 18,555–18,581, 1999b.

Liu, S. C., M. Trainer, F. C. Fehsenfeld, D. D. Parish, E. J. Williams, D. W. Fahey, G. Hubler, and P. C. Murphy, Ozone production in the rural troposphere and the implication of regional and global ozone distributions, *J. Geophys. Res.*, **92**, 4191–4207, 1987.

Marchuk, G. I., *Adjoint Equations and Analysis of Complex Systems*, Kluwer Acad., Norwell, Mass., 1995.

McKeen, S. A., M. Trainer, E. Y. Hsie, R. K. Tallamraju, and S. C. Liu, On the indirect determination of atmospheric OH radical concentrations from reactive hydrocarbon measurements, *J. Geophys. Res.*, **95**, 7493–7500, 1990.

Pickering, K. E., A. M. Thompson, J. R. Scala, W.-K. Tao, and J. Simpson, Ozone production potential following convective redistribution of biomass burning emissions, *J. Atmos. Chem.*, **14**, 297–313, 1992a.

Pickering, K. E., A. M. Thompson, J. R. Scala, W.-K. Tao, R. R. Dickerson, and J. Simpson, Free tropospheric ozone production following entrainment of urban plumes into deep convection, *J. Geophys. Res.*, **97**, 17,985–18,000, 1992b.

Pudykiewicz, J. A., Application of adjoint tracer transport equations for evaluating source parameters, *Atmos. Environ.*, **32**, 3039–3050, 1998.

Rabier, F., P. Courtier, and O. Talagrand, An application of adjoint

- models to sensitivity analysis, *Contrib. Atmos. Phys.*, **65**, 177–192, 1992.
- Ridley, B. A., E. L. Atlas, J. G. Walega, G. L. Kok, T. A. Staffelbach, J. P. Greenberg, F. E. Grahek, P. G. Hess, and D. D. Montzka, Aircraft measurements made during the spring maximum of ozone over Hawaii: Peroxides, CO, O₃, NO_x, condensation nuclei, selected hydrocarbons, halocarbons, and alkyl nitrates between 0.5 and 9 km altitude, *J. Geophys. Res.*, **102**, 18,935–18,961, 1997.
- Robertson, A. W., Diagnosis of regional monthly anomalies using the adjoint method, part I, Temperature, *J. Atmos. Sci.*, **49**, 885–905, 1992.
- Roe, P. L., and D. Sidilkover, Optimum positive linear schemes for advection in two and three dimensions, *SIAM J. Numer. Anal.*, **29**, 1542–1568, 1992.
- Smolarkiewicz, P. K., A fully multidimensional positive definite advection algorithm with small implicit diffusion, *J. Comput. Phys.*, **54**, 325–362, 1984.
- Smolarkiewicz, P., and L. G. Margolin, MPDATA: A finite-difference solver for geophysical flows, *J. Comput. Phys.*, in press, 1999.
- Vukićević, T., Nonlinear and linear evolution of initial forecast errors, *Mon. Weather Rev.*, **119**, 1602–1611, 1991.
- Vukićević, T., Optimal initial perturbations for two cases of extratropical cyclogenesis, *Tellus, Ser. A*, **50**, 143–166, 1998.
- Vukićević, T., and R. M. Errico, Linearization and adjoint of parameterized diabatic processes, *Tellus, Ser. A*, **45**, 493–510, 1993.
- Vukićević, T., and K. Raeder, Use of an adjoint model for finding triggers for Alpine lee cyclogenesis, *Mon. Weather Rev.*, **123**, 800–816, 1995.
- Wesely, M. L., Parameterization of surface resistance to gaseous dry deposition in regional-scale numerical models, *Atmos. Environ.*, **23**, 1293–1304, 1989.
- Zou, X., A. Barcilon, I. M. Navon, J. Whitaker, and D. G. Caccuci, An adjoint sensitivity study of blocking in a two-layer isentropic model, *Mon. Weather Rev.*, **121**, 2833–2857, 1993.
-
- P. Hess, National Center for Atmospheric Research, Boulder, CO 80302.
- T. Vukićević (corresponding author), CIRA, Colorado State University, Fort Collins, CO 80523-1375. (tomi@cira.colostate.edu)
- (Received April 21, 1999; revised October 11, 1999; accepted October 18, 1999.)